Uniformly Accurate Layered Medium Green's Function Approximation via Scattered Field Formulation of the Spectral Differential Equation Method

by

Xinbo Li

A thesis submitted to the Faculty of Graduate Studies of

The University of Manitoba

in partial fulfillment of the requirements for the degree of

Master of Science

Department of Electrical and Computer Engineering

Winnipeg, Manitoba, Canada

ABSTRACT

Evaluation of the multilayer medium Green's function is essential in many practical applications of electromagnetic analysis including the design of microwave circuits and microstrip antennas, modeling of high-speed interconnects, remote sensing, geoscience, and others. Expansion of the layered medium dyadic Green's function's components over cylindrical waves obtained through the finite-difference solution to 1D differential equation governing their spectra is an effective method to approximate the fields in the intermediate and far zones of the point source (Okhmatovski et al., IEEE TAP 2002). In the near vicinity of the point source, however, such approximation becomes inaccurate. This is due to spherical waves dominating the solution near the source and counted number of cylindrical waves becoming inadequate to their accurate description. To develop uniformly accurate approximation, we decompose the spectrum of the total potential into the incident and scattered potential contributions. The 1D differential equation governing the spectrum of the layered medium Green's function is formulated with respect to the scattered potential rather than the total potential as it was done previously (Okhmatovski et al., IEEE TAP 2002). The boundary conditions at dielectric layer interfaces, based on the continuity of the Green's function and the normal component of electric flux density are enforced. As a result, the pole-residual approximation of the scattered potential spectrum is obtained which leads to accurate cylindrical wave approximation in the spatial domain in both the intermediate and far zones since singularity of Green's function resides in the incident potential. The incident field is subsequently added in the analytic form and, hence, accurately describes the field near the source.

Acknowledgements

I would like to thank Dr. Vladimir Okhmatovski, my M.Sc. program advisor, for leading me into the fascinating computational electromagnetic world, and being innovative, supportive, and responsive in research work. I also want to thank Dr. Mohammed Al-Qedra, who was with the University of Manitoba and has done the prior work on higher-order finite element method research. His work was consulted in this research project. I have special thanks to Dr. Ian Jeffrey, for selflessly providing knowledge on forward solvers, continuous guidance, help, and attention in my research.

To Dr. Okhmatovski, Dr. Jeffrey, and My Family

Contents

List of Tables

List of Figures

List of Acronyms

MoM	Method of Moments
SI	Sommerfeld integral
DCIM	Discrete Complex Image Method
RFFM	Rational Function Fitting Method
SDEAM	Spectral Differential Equation Approximation Method
GPOF	Generalized Pencil of Function
PEC	perfect electric conductor
PDE	partial differential equation
ODE	ordinary differential equation
RHS	right hand side
LHS	left hand side
SLE	system of linear equations
FDM	Finite Difference Method
FEM	Finite Element Method
DGM	Discontinuous Galerkin Method
MAPE	mean absolute percentage error

List of Symbols

Operators

$\nabla\cdot$	Divergence operator.
∇	Curl operator.
$\mathcal{F}\{\}$	Fourier transform operator.
$\mathcal{F}^{-1}\{\}$	Inverse Fourier transform operator.
$\mathcal{FB}\{\}$	Fourier-Bessel transform operator.
$\mathcal{FB}^{-1}\{\}$	Inverse Fourier-Bessel transform operator.
∇^2	Laplace operator.

Geometry

ρ, ρ'	Radial distance to z axis in cylindrical coordinate system of the observation point and source, respectively.
λ	Radial coordinate in Fourier transformed k-space.
z, z'	z coordinate of the observation point and source, respectively.
ϕ	Angle between the reference direction on the $z = 0$ plane and the line from the origin to the projection of observation point on the plane.
d	Total length of medium in z direction between PEC walls.
$\mathbf{r}$, $\mathbf{r}'$	Position vector of the observation point and source, respectively.
h	Length of each element in finite element discretization.

Physical Quantities and Functions

ϵ_0	Permittivity of free space.
ϵ_r	Relative permittivity.

ϵ_i	Permittivity in ith layer.
ϵ_{src}	Permittivity in source layer.
$\epsilon^{(e)}$	Permittivity in eth element.
ρ_p	Volume charge density of the point charge source.
$\mathbf{E}$	Electric field.
$\mathbf{D}$	Electric flux density.
φ	Electric potential.
G	Spatial domain Green's function.
$\tilde{G}$	Spectral domain Green's function. When used with subscript i, means Green's function in ith layer.
G_0, $\tilde{G}_0$	Spatial domain and spectral domain incident Green's function, respectively.
F, $\tilde{F}$	Spatial domain and spectral domain scattered Green's function, respectively.

Mathematical Quantities and Functions

$\delta(x)$	Dirac delta.
$\delta_{nn'}$	Kronecker delta.
J_0	Bessel function of first kind with order zero.
$H_\nu^{(1)}, H_\nu^{(2)}$	Hankel function of first kind and second kind with order ν.
$S_p^{(e)}$	The pth shape function of eth element.
i	Imaginary unit except for when used as subscript.
C	Coefficient, used with or without subscript.
$\mathrm{sgn}(x)$	Sign function.
N_e	Number of elements in FEM.
N_l	Number of layers.
N_{int}	Number of interfaces.

Chapter 1

Introduction

1.1 Background and Motivation

The multilayer media structures are found in the substrates of integrated circuits [1] and optical devices [2], as the soil models in the design of grounding systems of power installations [3], as the stratifications of the earth layers [4] and/or ice layers [5] in geoscience, and many other practical scenarios. For this reason, the analysis of electromagnetic fields in multilayer media plays an important role in various areas of engineering and science.

Integral equations of electromagnetics [6] have been particularly popular in analysis of scattering and radiation problems in multilayer media. They allow us to decompose such problems into the problem of determining the Green's function [7, 8] of the appropriate layered medium and the problem of Method of Moments (MoM) [9] discretization of the pertinent integral equations with such Green's function. This decomposition of the original problem substantially simplifies the MoM solution and reduces its matrix equation size since the MoM is required to discretize only the object of interest and not the layers of the stratified medium it is embedded into. The accuracy of such MoM solutions, however, critically depends

on accurate evaluation of its basis and test functions interactions in the presence of multilayer medium, which substantially complicates both the physics of the involved electromagnetic fields and the procedures for their numerical evaluation. These procedures include computation of the Green's functions and interpolation of its values in the process of MoM reaction integrals computation.

Green's functions can be constructed efficiently only for time-harmonic analysis in canonical layered media configurations (e.g., infinite planar, spherical, cylindrical, etc.) [8]. The accurate computation of the Green's functions in both the near and intermediate zones of the source radiating in a general non-canonical multilayer medium has been a particularly challenging problem. It was a subject of intensive researches in both mathematical and engineering community over the past century [10–15]. The traditional approach to the computation of layered medium Green's functions has been through analytical solutions for their spectra which is followed by evaluation of the inverse Fourier transform (a.k.a. Sommerfeld Integrals (SI)) [8]. Due to complicated structures of the spectra, however, the SI's can only be computed numerically. Such numerical approach is time consuming especially when the spectrum of the Green's function is not attenuating rapidly (e.g. due to the presence of thin layers).

While there have been effective methods developed for acceleration of the convergence in the integrands of the SIs and their rapid evaluation [16, 17], techniques approximating the Green's function's spectra with pole-residual form or complex exponentials have been offering an inexpensive and often sufficiently accurate alternative. Among such methods are the Discrete Complex Image Method (DCIM) [18–20], the Rational Function Fitting Method (RFFM) [21, 22], and the Spectral Differential Equation Approximation Method (SDEAM) [23–25]. The DCIM is the most popular of these approaches. It approximates the spectrum of the Green's function with complex exponentials using the Generalized Pencil of Function (GPOF) method [26]. The form of the fitting exponential functions is

such that the SI from each of them can be evaluated analytically and produce a spherical wave function (image) emanating from a complex location in the spatial domain. Such spherical waves approximate the field near the point source very accurately. However, far from the source where the field in layered medium is typically dominated by cylindrical wave contributions, they typically fail to provide any reasonable approximation unless a large number of images is taken [27] which is computationally expensive.

The RFFM and SDEAM approximate the field of a point source in layered media with a series of Hankel functions which correspond to the cylindrical waves emanating from the source. Such superposition of the cylindrical waves accurately approximates the field of a point source in layered media far away from the source as well as in the intermediate region. However, near the source, where the field is dominated by the spherical waves, the solution requires the larger number of the cylindrical waves terms, the closer the observer approaches the source point location. Indeed, an infinite number of cylindrical waves is required to represent the field of spherical waves at the location of the source. The transitions between the near field region, intermediate region, and far field region are not clearly defined. They are case dependent with the thickness of the layers, location of the source with respect to the dielectric interfaces, material parameters, and other factors determining the transitions. For that reason, it is difficult to provide a uniformly accurate approximation of the layered medium Green's functions in general media for all distances of interest. Typically, accurate near field approximation is obtained with DCIM, while the accurate far field approximation is obtained with RFFM or DCIM applied to the spectra after dominant far field contributors (e.g., surface waves) have been extracted from them [18]. Because the systematic combining of the near and far field solutions has proven to be difficult in general practical cases, expensive direct numerical evaluation of the SI's is used

to provide robust uniform approximations. This motivates the search for alternative approaches allowing to obtain accurate uniform approximations of the layered media Green's function which can be both accurate, robust, and inexpensive.

1.1.1 Contribution

In this work, we present a proof of concept for a new method which allows performing uniformly accurate Green's function evaluation in planar stratified multilayer medium. To simplify the introduction of the new method, the case of electrostatic Green's function of a planar layered medium bounded with perfect electric conductor (PEC) planes at the top and the bottom of the layer stack is considered. We refer to this method as *the scattered field formulation of the SDEAM*. Scattered field formulation has been widely used in computational electromagnetics in both the finite element and the finite difference methods for solutions of general problems of radiation and scattering. In such scattered field formulations, the differential equations (e.g., curl-curl equation or Helmholtz equation) are stated with respect to the scattered field instead of the total field, the former being the difference of the unknown total field and a conveniently chose known incident field.

Following the same principle in this work, we introduce the scattered field formulation into the SDEAM. Specifically, we decompose the Green's function into the incident and scattered field contributions and state pertinent differential equations with respect to the scattered field instead of the total field. As for the incident field, we utilize the accurately obtained analytical expression for the Green's function of the simpler medium than the layered medium of the original problem (e.g., Green's function of the parallel plate waveguide). The scattered contribution part is subsequently computed numerically using properly formulated SDEAM. In the vicinity of the source, the incident Green's function dominates the total Green's function. Thus, accurate incident Green's function guarantees accurate

total Green's function approximation near the source. When the observation is far from the source, the Hankel functions superposition resultant from SDEAM gives accurate Green's function approximation far from the source. The proposed scattered field formulation of the SDEAM, hence, provides uniformly accurate Green's function approximation in the near, intermediate, and far zones. When the number of layers is not too large, the computational cost of scattered field SDEAM is comparable to the conventional total field formulation of SDEAM, which solves for the Green's function's total field directly.

1.1.2 Organization of thesis

The following work is organized as in Section 1.2, the geometry of the PEC covered planar stratified radial symmetric multilayer medium is stated. The Green's function evaluation problem is posed in this medium geometry. The reason and approach to go from the spatial domain in which the problem is posed, to the spectral domain where the problem is solved, are explained in Section 1.2.2. In Chapter 2, the spectral domain analytical solutions to total field and incident field are derived. The scattered field formulation proposed in this work is explained in Chapters 3 and 4. Scattered field's spectrum is solved numerically in Chapter 3. Finally, the spatial domain Green's function, which is of interest, is recovered by adding scattered field and incident field in Chapter 4. The new method is summarized in Chapter 5.

1.2 Problem Statement

For a PEC bounded multilayer medium and an assumed cylindrical system (ρ, ϕ, z), a unit point charge is located at $(0, 0, z')$, acting as the source. The Green's function $G(\rho, z; z')$, which is the scalar filed as impulse response stimulated by the

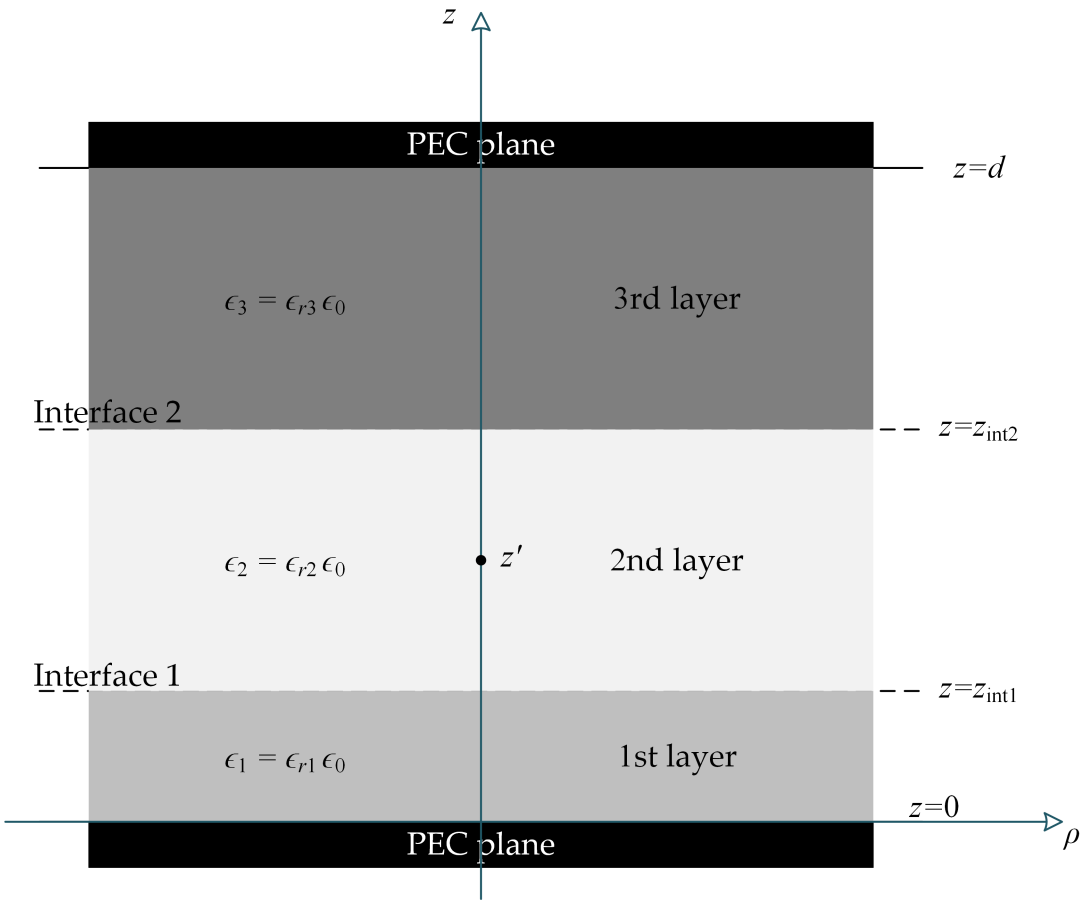

FIGURE 1.1: Multilayer Medium Green's Function Evaluation Problem

point source, is of interest. The Green's function we are solving for has a meaning of electric potential. The terms "Green's function", "potential", and "field", however, are used interchangeably in the sequel, For example, the term "incident field" is used interchangeably with the term "incident potential" or "incident Green's function". Figure 1.1 shows a three-layer medium where the bottom PEC plane is set as $z = 0$ and top PEC plane has $z = d$ where d is the distance between the top and bottom PEC planes. To simplify the analysis, the medium is considered to have piece-wise constant permittivity, thus, homogeneous in each layer. Within each layer, the medium is also assumed to be linear, homogeneous, and isotropic.

1.2.1 Poisson's Equation for Green's Function

Gauss's law in differential form gives [28]

$$\nabla \cdot \mathbf{D} = \rho_p, \tag{1.1}$$

where $\mathbf{D}$ is the electric flux density (C/m^2) and ρ_p is the point source volume charge density (C/m^3). Based on the constitutive relationship between electric flux density $\mathbf{D}$ and electric field $\mathbf{E}$ [28]

$$\mathbf{D} = \epsilon \mathbf{E}, \tag{1.2}$$

and the fact that

$$\mathbf{E} = -\nabla \varphi, \tag{1.3}$$

where φ is the scalar electric potential, we have

$$\nabla \cdot (\epsilon(-\nabla \varphi)) = \rho_p. \tag{1.4}$$

For a point source with unit charge, the charge density is represented by Dirac delta function as [8]

$$\rho_p = \delta(\mathbf{r} - \mathbf{r}'), \tag{1.5}$$

where $\mathbf{r}$ and $\mathbf{r}'$ are position vectors of the observation and source points, respectively. Vector $\mathbf{r}$ has length r defined by Euclidean norm $r = \sqrt{\rho^2 + z^2}$, it points from the origin to the point of observation. Similarly, $\mathbf{r}'$ has length $r' = \sqrt{(\rho')^2 + (z')^2}$, pointing from the origin to the point source. In the particular case we discuss in this whole document, $\rho' = 0$. Hence, (1.5) becomes [8]

$$\rho_p = \frac{\delta(\rho)}{2\pi\rho}\delta(z - z'), \tag{1.6}$$

in the cylindrical coordinate system. Plugging (1.6) into (1.4), we have

$$\nabla^2\varphi = -\frac{\delta(\rho)}{2\pi\rho\epsilon}\delta(z - z'), \tag{1.7}$$

in each dielectric layer. The divergence operator does not operate on ϵ because it is assumed to be a constant within each layer.

Since the Green's function has the physical meaning of electric potential due to a unit point source, φ in (1.7) is substituted with G, resulting in Poisson's equation governing Green's function

$$\nabla^2 G = -\frac{1}{\epsilon}\frac{\delta(\rho)}{2\pi\rho}\delta(z - z'). \tag{1.8}$$

This partial differential equation (PDE) is hard to solve directly in the spatial domain. In Section 1.2.2, the PDE is cast into the spectral domain with the help of SI in order to enable its subsequent evaluation in the spatial domain.

1.2.2 Spectral Domain Boundary Value Problem

The Green's function in above mentioned multilayer medium is does not have dependence on ϕ when the point charge is located on z axis ($\rho' = 0$) because of the circular symmetry property of the layered medium. The 2D Fourier transform is then the Fourier-Bessel transform where integration over ϕ is carried out. The Fourier-Bessel transform projects functions in three-dimensional Euclidean space to corresponding functions in so called spectral domain. In spectral domain, (1.8) is converted into a one-dimensional ordinary differential equation (ODE) which is

easier to solve. The Fourier-Bessel transform pair is given as [8]

$$\tilde{G}(\lambda, z; z') = \int_0^\infty G(\rho, z; z') J_0(\lambda\rho)\rho d\rho, \tag{1.9}$$

$$G(\rho, z; z') = \int_0^\infty \tilde{G}(\lambda, z; z') J_0(\lambda\rho)\lambda d\lambda, \tag{1.10}$$

where G and $\tilde{G}$ are Green's functions in the spatial and spectral domain, respectively. Variable λ is the radial coordinate in transformed k-space. The Bessel function of the first kind with order zero, J_0, satisfies

$$J_0(\lambda\rho) = \frac{1}{2\pi}\int_{\theta=0}^{2\pi} e^{i\lambda\rho\cos\theta} d\theta. \tag{1.11}$$

The Fourier transform in the polar system of $\delta(\rho)/(2\pi\rho)$ on the right hand side (RHS) of (1.8) satisfies

$$\mathcal{F}\left\{\frac{\delta(\rho)}{2\pi\rho}\right\} = \int_{\phi=0}^{2\pi} d\phi \int_{\rho=0}^{\infty} \frac{\delta(\rho)}{2\pi\rho} e^{-i\lambda\rho\cos(\alpha-\phi)}\rho d\rho = 1, \tag{1.12}$$

where α is the angular coordinate of the polar system in the transformed k-space, $\mathcal{F}\{\}$ is the Fourier transform operator. The Cartesian coordinates before and after the Fourier transform are listed as (1.13) and (1.14) for better understanding

$$x = \rho\cos\phi \underset{\mathcal{F}^{-1}}{\overset{\mathcal{F}}{\rightleftharpoons}} k_x = \lambda\cos\alpha, \tag{1.13}$$

$$y = \rho\sin\phi \underset{\mathcal{F}^{-1}}{\overset{\mathcal{F}}{\rightleftharpoons}} k_y = \lambda\sin\alpha. \tag{1.14}$$

In this work, the cylindrical coordinate system is used for volumes, and polar coordinate system is used for planes.

Given (1.12), the RHS of (1.8), $\delta(\rho)/(2\pi\rho)$, can be represented by its inverse Fourier transform, which is equal to number 1 [8] :

$$\frac{\delta(\rho)}{2\pi\rho} = \mathcal{F}^{-1}\{1\} = \frac{1}{(2\pi)^2}\int_{\lambda=0}^{\infty}\lambda d\lambda\int_{\alpha=0}^{2\pi}e^{i\lambda\rho\cos(\alpha-\phi)}d\alpha = \frac{1}{2\pi}\int_{\lambda=0}^{\infty}J_0(\lambda\rho)\lambda d\lambda. \tag{1.15}$$

In terms of the LHS of (1.8), based on inverse Fourier transform of $\tilde{G}$, Laplacian operating on G can be represented as [8]

$$\nabla^2 G = \left(\frac{\partial^2}{\partial x^2}+\frac{\partial^2}{\partial y^2}+\frac{\partial^2}{\partial z^2}\right)\frac{1}{(2\pi)^2}\iint\limits_{k_x,k_y=-\infty}^{\infty}\tilde{G}(k_x,k_y,z;z')e^{i(k_x x+k_y y)}dk_x dk_y, \tag{1.16}$$

$$= \frac{1}{(2\pi)^2}\iint\limits_{k_x,k_y=-\infty}^{\infty}\left(-k_x^2-k_y^2+\frac{d^2}{dz^2}\right)\tilde{G}(k_x,k_y,z;z')e^{i(k_x x+k_y y)}dk_x dk_y \tag{1.17}$$

$$= \frac{1}{(2\pi)^2}\int_{\lambda=0}^{\infty}\left(-\lambda^2+\frac{d^2}{dz^2}\right)\tilde{G}(\lambda,z;z')\left(\int_{\alpha=0}^{2\pi}e^{i\lambda\rho\cos(\alpha-\phi)}d\alpha\right)\lambda d\lambda \tag{1.18}$$

$$= \frac{1}{2\pi}\int_{\lambda=0}^{\infty}\left(-\lambda^2+\frac{d^2}{dz^2}\right)\tilde{G}(\lambda,z;z')J_0(\lambda\rho)\lambda d\lambda. \tag{1.19}$$

As a result, we have the equivalent form of (1.8) as

$$\int_{\lambda=0}^{\infty}\left(-\lambda^2+\frac{d^2}{dz^2}\right)\tilde{G}(\lambda,z;z')J_0(\lambda\rho)\lambda d\lambda = \int_{\lambda=0}^{\infty}-\frac{1}{2\pi\epsilon}\delta(z-z')J_0(\lambda\rho)\lambda d\lambda. \tag{1.20}$$

That is,

$$\mathcal{F}\mathcal{B}^{-1}\left\{\left(-\lambda^2+\frac{d^2}{dz^2}\right)\tilde{G}(\lambda,z;z')\right\} = \mathcal{F}\mathcal{B}^{-1}\left\{-\frac{1}{2\pi\epsilon}\delta(z-z')\right\}. \tag{1.21}$$

Then we have

$$\frac{d^2}{dz^2}\tilde{G}(\lambda,z;z') - \lambda^2\tilde{G}(\lambda,z;z') = -\frac{1}{2\pi\epsilon}\delta(z-z'), \tag{1.22}$$

based on the following lemma and corollary, whose proofs can be found in Appendix A.

Lemma 1.1. *Two functions having identical spectra after Fourier transform are identical.*

Corollary 1.2. *Two functions with identical Fourier-Bessel transform are identical.*

Equation (1.22) is an ODE since, for a given z' and λ, $\tilde{G}$ is a function of z while only the derivative over z exists in the equation [29]. We have (1.22) as the one-dimensional spectral domain ODE representation of original three-dimensional PDE (1.8) in the spatial domain. The decrease in dimensions brings down the difficulty to solve the PDE dramatically.

Due to vanishing electric potential on PEC planes, $G|_{z=0} = 0$, $G|_{z=d} = 0$. After applying Fourier-Bessel transform, $\tilde{G}|_{z=0} = 0$ and $\tilde{G}|_{z=d} = 0$ are the boundary conditions for the spectral domain boundary value problem (BVP). The BVP was solved using the Finite Difference Method (FDM) in [29]. The Green's function's spectrum $\tilde{G}$ obtained was in pole residual form. The spatial domain G was recovered by performing inverse Fourier-Bessel transform analytically on each term in the pole residual form of $\tilde{G}$. The inverse Fourier-Bessel transform returns G as a superposition of Hankel functions. However, since Hankel functions are used to represent outward- and inward-propagating cylindrical-wave, they struggle to grasp the nature of the spherical wave behavior of Green's function in the vicinity of the source. Thus the solution is inaccurate in the near-source region. This non-accurate near field will be shown later in the numerical results discussion in Chapter 4.

To solve this problem, we propose a new method that separates the incident field (named as $\tilde{G}_0$ in the spectral domain, G_0 in the spatial domain) and scattered field

(denoted as $\tilde{F}$ in the spectral domain, F in the spatial domain). The new method will be referred to as scattered field formulation later in this text. The scattered field is determined numerically in the spectral domain, while the incident field is calculated analytically. The dominant incident field in the near-source region captures the spherical wave behavior. Hence the total Green's function result is more accurate near the source. In the far zone, Hankel functions represented scattered field and analytically obtained accurate incident field can recover the total Green's function accurately as well. As a result, the scattered field formulation yields desired uniformly accurate approximation of the sought Green's function.

Chapter 2

Analytical Solutions in Spectral Domain

In this chapter, the analytical solutions to total potential and incident potential in the spectral domain are derived. The spectral domain incident potential analytical solution will be subsequently transformed to the spatial domain and used when formulating spatial domain total potential. The analytical solution to total potential is used as the standard to validate the total potential evaluated numerically in the spectral domain.

2.1 Preliminary — Green's Function in Free Space

We first derive the Green's function for a point source located in free space. In free space, the ODE (1.22) is the only condition the Green's function needs to satisfy. No additional boundary conditions are required. To solve this ODE, we first seek the solution to the homogeneous equation

$$\frac{d^2\tilde{G}_h}{dz^2} - \lambda^2\tilde{G}_h = 0. \tag{2.1}$$

Based on characteristic equation [30] of (2.1), the solution should be in the form of

$$\tilde{G}_h(z) = C_1 e^{\lambda z} + C_2 e^{-\lambda z}, \tag{2.2}$$

where C_1 and C_2 are coefficients, which are functions of λ. This form of solution to the homogeneous equation indicates the original inhomogeneous equation (1.22) should have a solution in the form of exponentials and second derivative yielding delta function. The form [8]

$$\tilde{G} = Ce^{-\lambda|z-z'|} \tag{2.3}$$

satisfies both conditions since

$$\frac{d^2|z-z'|}{dz^2} = 2\delta(z-z'). \tag{2.4}$$

The reason why only negative power of exponential persists is because $\tilde{G} \to 0$ as $z \to \pm\infty$. Notice the first and second derivatives of (2.3) are

$$\frac{d\tilde{G}}{dz} = -C\lambda \text{sgn}(z-z')e^{-\lambda|z-z'|}, \tag{2.5}$$

$$\frac{d^2\tilde{G}}{dz^2} = -2C\lambda\delta(z-z')e^{-\lambda|z-z'|}. \tag{2.6}$$

Now plugging the derivatives back into (1.22) and integrating both sides of the equation over small vicinity of z' in interval $[z'-\delta z, z'+\delta z]$ where $\delta z \to 0$, we have

$$-2C\lambda \int_{z'-\delta z}^{z'+\delta z} \delta(z-z')e^{-\lambda|z-z'|}dz - \lambda^2 C \int_{z'-\delta z}^{z'+\delta z} e^{-\lambda|z-z'|}dz = -\frac{1}{2\pi\epsilon_0}\int_{z'-\delta z}^{z'+\delta z} \delta(z-z')dz. \tag{2.7}$$

This yields

$$-2C\lambda = -\frac{1}{2\pi\epsilon_0}, \tag{2.8}$$

which produces sought value of C

$$C = \frac{1}{4\pi\epsilon_0\lambda}. \tag{2.9}$$

In conclusion, the free space spectral domain Green's function is [8]

$$\tilde{G} = \frac{1}{4\pi\epsilon_0\lambda}e^{-\lambda|z-z'|}. \tag{2.10}$$

2.2 Analytical Total Potential — Green's Function in PEC Planes Bounded Multilayer Medium

2.2.1 Derivation

With spectral domain free space Green's function ready, we can expand it into Green's function of PEC planes bounded multilayer medium. Depending on the locations of dielectric layers, which affect the boundary conditions, and source location z', which affects the ODE (1.22), the solution to the BVP changes. To illustrate, consider the aforementioned three-layer case, as shown in Figure 1.1.

Denote spectral domain Green's function in ith layer as $\tilde{G}_i$. For layer 1 and layer 3, $\tilde{G}$ must satisfy

$$\frac{d^2\tilde{G}}{dz^2} - \lambda^2\tilde{G} = 0, \tag{2.11}$$

since the source is not in these layers. As shown in (2.2), the corresponding solutions to homogeneous ODE are thus

$$\tilde{G}_1 = C_{11}e^{-\lambda z} + C_{12}e^{\lambda z}, \tag{2.12}$$

and

$$\tilde{G}_3 = C_{31}e^{-\lambda z} + C_{32}e^{\lambda z}. \tag{2.13}$$

For layer 2, $\tilde{G}$ is under constraint of

$$\frac{d^2\tilde{G}}{dz^2} - \lambda^2\tilde{G} = -\frac{1}{2\pi\epsilon_2}\delta(z - z'). \tag{2.14}$$

The solution in layer 2, $\tilde{G}_2$ is in the form of

$$\tilde{G}_2 = \frac{1}{4\pi\epsilon_2\lambda}e^{-\lambda|z-z'|} + C_{21}e^{-\lambda z} + C_{22}e^{\lambda z}, \tag{2.15}$$

where the first term is the contribution from the presence of source. Notice that this term is in the same form as the free space solution (2.10). The second term is the wave emanating in positive z direction and reflected by the interface 1. The final term is the wave propagating in the negative z direction and reflected by the interface 2 as in Figure 1.1.

To find the unknown coefficients in front of the exponential functions in (2.12), (2.13), and (2.15), we enforce boundary conditions. The three types of boundary conditions needed are the continuity of the Green's function at dielectric interfaces, the continuity of normal component of the electric flux density at the interfaces, and the PEC vanishing potential conditions.

At interface 1, the potential continuity condition is

$$G_1\Big|_{z_{\text{int1}}} = G_2\Big|_{z_{\text{int1}}}. \tag{2.16}$$

The Fourier-Bessel transform converts (2.16) into the spectral domain as

$$\tilde{G}_1\Big|_{z_{\text{int1}}} = \tilde{G}_2\Big|_{z_{\text{int1}}}, \tag{2.17}$$

The normal component of electric flux density is continuous at interface 1 since no surface charge exists there:

$$(\mathbf{D}^-\big|_{\text{int1}} - \mathbf{D}^+\big|_{\text{int1}}) \cdot \mathbf{n}_{\text{int1}} = \sigma_s = 0, \tag{2.18}$$

where $\mathbf{D}^-$ and $\mathbf{D}^+$ are electric flux density below and above interface 1 respectively. The normal vector $\mathbf{n}_{\text{int1}}$ is pointing from z^-_{int1} to z^+_{int1}. Equation (2.18) can be written as

$$\epsilon_1 \frac{dG_1}{dz}\bigg|_{z=z_{\text{int1}}} = \epsilon_2 \frac{dG_2}{dz}\bigg|_{z=z_{\text{int1}}}, \tag{2.19}$$

since Green's function is treated as the electric potential. The Fourier-Bessel transform preserves derivative, so in the spectral domain

$$\epsilon_1 \frac{d\tilde{G}_1}{dz}\bigg|_{z=z_{\text{int1}}} = \epsilon_2 \frac{d\tilde{G}_2}{dz}\bigg|_{z=z_{\text{int1}}}. \tag{2.20}$$

Similarly, at interface 2, we have two types of boundary conditions as

$$\tilde{G}_2\Big|_{z=z_{\text{int2}}} = \tilde{G}_3\Big|_{z=z_{\text{int2}}}, \tag{2.21}$$

$$\epsilon_2 \frac{d\tilde{G}_2}{dz}\bigg|_{z=z_{\text{int2}}} = \epsilon_3 \frac{d\tilde{G}_3}{dz}\bigg|_{z=z_{\text{int2}}}. \tag{2.22}$$

At the PEC planes, the vanishing potential boundary conditions are

$$\tilde{G}_3\Big|_{z=d} = 0, \tag{2.23}$$

$$\tilde{G}_1\Big|_{z=0} = 0. \tag{2.24}$$

The above boundary conditions introduce six equations which are necessary for determining the six unknown coefficients C_{11} through C_{32} in (2.12), (2.13), and (2.15). Once the coefficients are obtained, we have the analytical spectral domain Green's function for multilayer medium. The three-layer case can be generalized to an arbitrary number of layers case. In general, we have $2N_l$ unknown coefficients and $2N_l$ equations from boundary conditions for N_l layers medium. The analytical expressions for the coefficients are complicated functions with dependences on λ. Therefore, the SI of spectral-domain analytical Green's function to the spatial domain can not be readily performed analytically.

2.2.2 Illustration

For illustration purpose, the behavior of the analytical total Green's function $\tilde{G}$ as z varies in a three-layer medium specified in Figure 2.1 can be found in Figure 2.2. The total distance between PEC planes d is chosen as 1 mm. Bottom PEC plane is put at $z_{\min} = 0$ mm, so top PEC plane is at $z_{\max} = 1$ mm. Dielectric interfaces are set at z_{int1} =0.2 mm and z_{int2} =0.6 mm. Point source is put at z' =0.4 mm. The relative permittivity for three layers are $\epsilon_{r1} = 5$, $\epsilon_{r2} = 1$, and $\epsilon_{r3} = 10$.

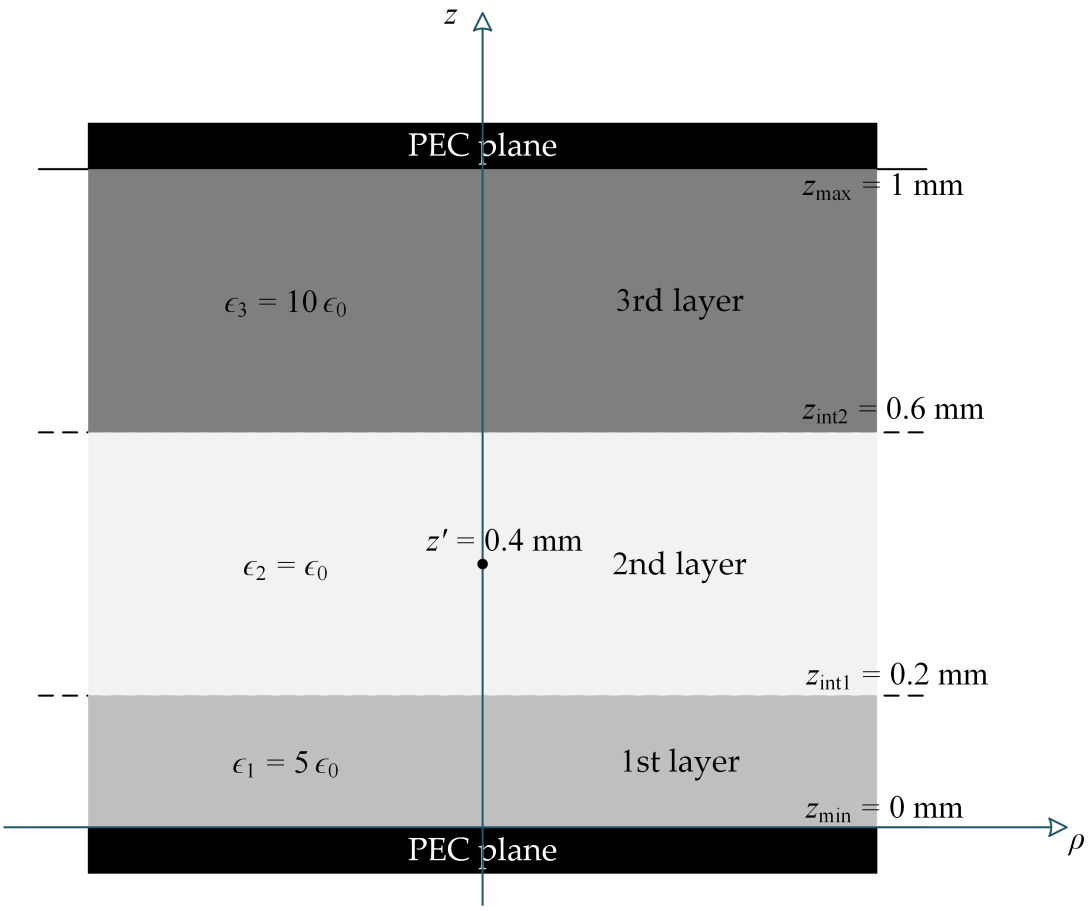

FIGURE 2.1: Multilayer Medium Problem Specification

Spectral domain parameter λ is fixed at 100, 1000, 5000, 10 000 m^{-1} rad in the plots. One can notice that spectral domain Green's function is differentiable in $(0, d)$ except for at dielectric interfaces and point charge. Green's function's spectrum reaches peak value at the point charge location.

2.3 Incident Potential — PEC Planes Bounded Homogeneous Medium Solution

Consider homogeneous medium bounded by PEC planes which has the same distance between PEC planes as in the multilayer medium. The permittivity of this

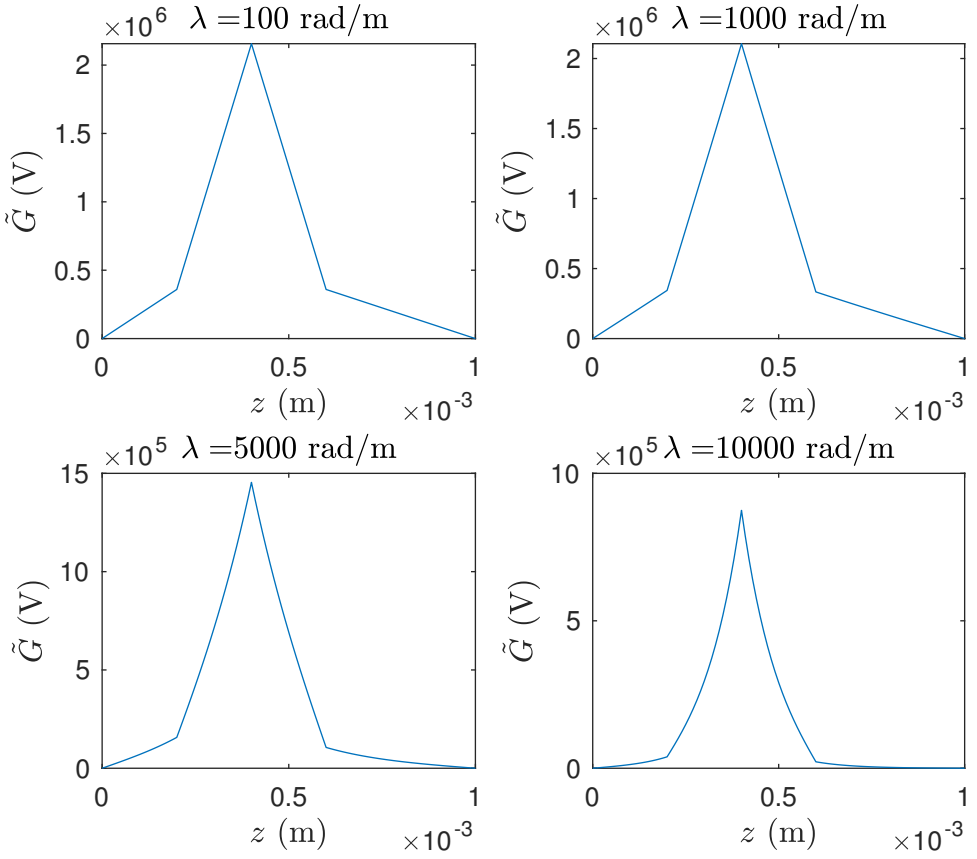

FIGURE 2.2: Spectral Domain Analytically Obtained Green's Function $\tilde{G}$ Behavior

homogeneous medium is the permittivity in the source layer of corresponding multilayer medium. The geometry of the medium corresponding to the aforementioned three-layer case in Figure 1.1 is shown in Figure 2.3, where $\epsilon_{\text{src}} = \epsilon_2$.

The particular Green's function in this homogeneous medium is the result of the presence of source and PEC walls without the multilayer structure of the medium. It is named as the incident potential (referred to as $\tilde{G}_0$ in the spectral domain, G_0 in the spatial domain). Being the same as in (2.15), to represent the source contribution and PEC planes reflected waves, $\tilde{G}_0$ is in the form of

$$\tilde{G}_0 = \frac{1}{4\pi\epsilon_{\text{src}}\lambda} e^{-\lambda|z-z'|} + C_1 e^{-\lambda z} + C_2 e^{\lambda z}. \tag{2.25}$$

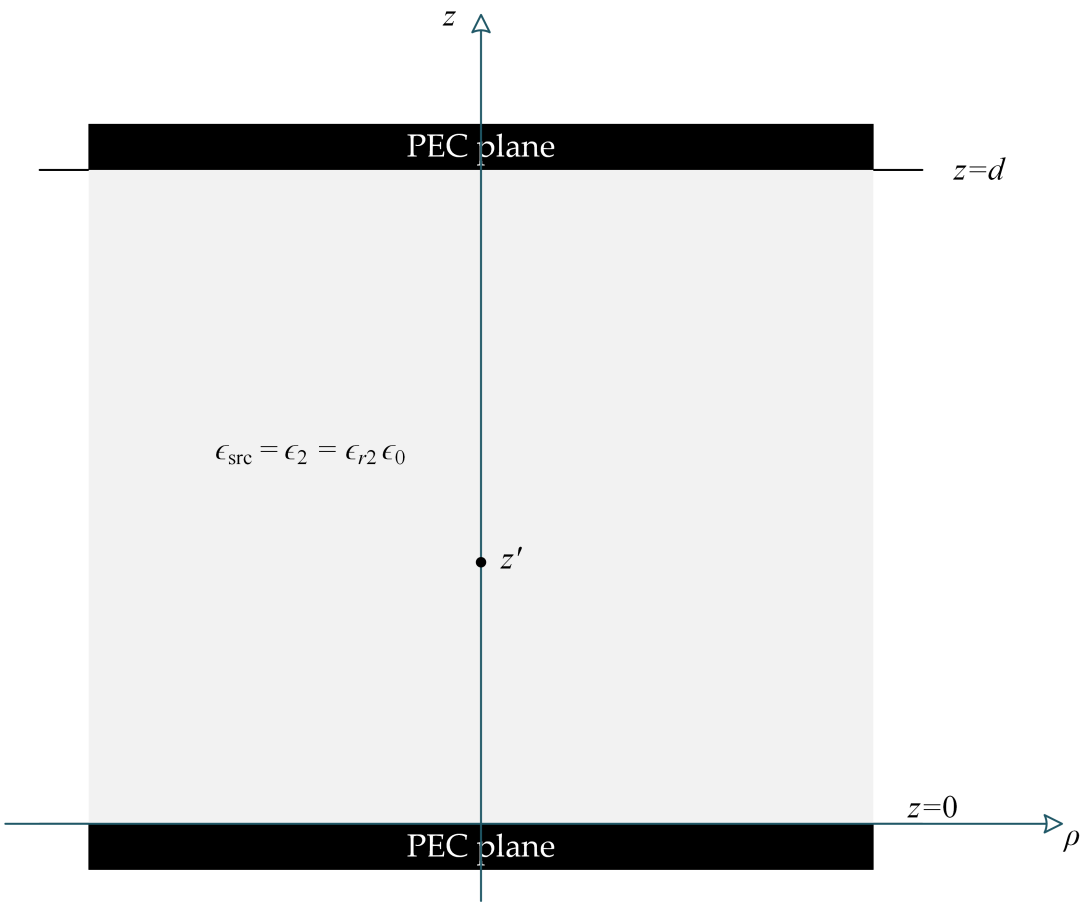

FIGURE 2.3: Homogeneous Medium for Evaluating Incident Green's Function

Coefficients C_1 and C_2 are obtained by enforcing the potential vanishing boundary conditions at PEC planes as $\tilde{G}_0|_{z=0} = \tilde{G}_0|_{z=d} = 0$. This closed-form expression is accurate and is used to recover total potential once scattered potential is obtained numerically. However, the coefficients C_1 and C_2 are complicated functions of λ:

$$C_1 = -\frac{e^{\lambda(d-z')} - e^{-\lambda(d-z')}}{4\pi\epsilon_{\text{src}}\lambda(e^{\lambda d} - e^{-\lambda d})}, \tag{2.26}$$

$$C_2 = \frac{e^{-\lambda(d+z')} - e^{-\lambda(d-z')}}{4\pi\epsilon_{\text{src}}\lambda(e^{\lambda d} - e^{-\lambda d})}, \tag{2.27}$$

so it is hard to perform inverse Fourier-Bessel transform on (2.25). This causes difficulty for the spatial domain incident potential derivation. To address this

issue, we then derive the analytical parallel plate waveguide modes representation of the incident potential.

Based on separation of variables [31], $\tilde{G}_0$ is sought as a solution that is not identically zero satisfying the boundary conditions with dependencies on λ and z separated [32], that is,

$$\tilde{G}_0 = \Lambda(\lambda)Z(z). \tag{2.28}$$

We choose $Z(z)$ as sine, the eigenfunction of the 2nd order derivative operator satisfying the boundary conditions. Then we can expand $\tilde{G}_0$ in terms of sine Fourier series as

$$\tilde{G}_0 = \sum_{n=1}^{\infty} \Lambda_n(\lambda) \sin\left(\frac{n\pi z}{d}\right), \tag{2.29}$$

since $\left\{\sin\frac{n\pi z}{d}\right\}_{n=1}^{\infty}$ is an orthogonal and complete set of bases. To find coefficients $\Lambda_n(\lambda)$ of the harmonics, we substitute (2.29) back to (1.22) and have

$$\left(\left(\frac{n\pi}{d}\right)^2 + \lambda^2\right) \sum_{n=1}^{\infty} \Lambda_n(\lambda) \sin\left(\frac{n\pi z}{d}\right) = \frac{1}{2\pi\epsilon_{\text{src}}}\delta(z - z'). \tag{2.30}$$

To solve for the n'th coefficient, we use the orthogonality of sine harmonics by multiplying both sides of (2.30) with $\sin(n'\pi z/d)$, then integrate both sides from 0 to d:

$$\begin{aligned}\left(\left(\frac{n\pi}{d}\right)^2 + \lambda^2\right) \sum_{n=1}^{\infty} \Lambda_n(\lambda) \int_{z=0}^{d} \sin\left(\frac{n\pi z}{d}\right) \sin\left(\frac{n'\pi z}{d}\right) dz \\ = \frac{1}{2\pi\epsilon_{\text{src}}} \int_{z=0}^{d} \delta(z - z') \sin\left(\frac{n'\pi z}{d}\right) dz.\end{aligned} \tag{2.31}$$

This yields

$$\left(\left(\frac{n\pi}{d}\right)^2 + \lambda^2\right) \sum_{n=1}^{\infty} \Lambda_n(\lambda) \frac{d}{2}\delta_{nn'} = \frac{1}{2\pi\epsilon_{\text{src}}} \sin\left(\frac{n'\pi z'}{d}\right), \tag{2.32}$$

where $\delta_{nn'}$ is Kronecker delta. The sifting property of Kronecker delta gives

$$\Lambda_{n'}(\lambda) = \frac{1}{\pi\epsilon_{\text{src}}d}\sin\left(\frac{n'\pi z'}{d}\right)\frac{1}{\left(\frac{n'\pi}{d}\right)^2+\lambda^2}. \tag{2.33}$$

Once coefficients Λ are obtained in (2.33), we have $\tilde{G}_0$ as expansion of sine harmonics as [32]

$$\tilde{G}_0 = \frac{1}{\pi\epsilon_{\text{src}}d}\sum_{n=1}^{\infty}\sin\left(\frac{n\pi z}{d}\right)\sin\left(\frac{n\pi z'}{d}\right)\frac{1}{\left(\frac{n\pi}{d}\right)^2+\lambda^2}. \tag{2.34}$$

The pole residual form in (2.34) facilitates applying inverse Fourier-Bessel transform to evaluate spatial domain G_0 analytically.

Analytical results for incident potential in the spectral domain $\tilde{G}_0$ is illustrated in Figure 2.4. The medium specification is the same as what is used for total potential $\tilde{G}$. Since incident potential is Green's function for homogeneous medium, $\tilde{G}_0$ is differentiable in $(0, d) \setminus \{z'\}$ where $\setminus$ means set subtraction.

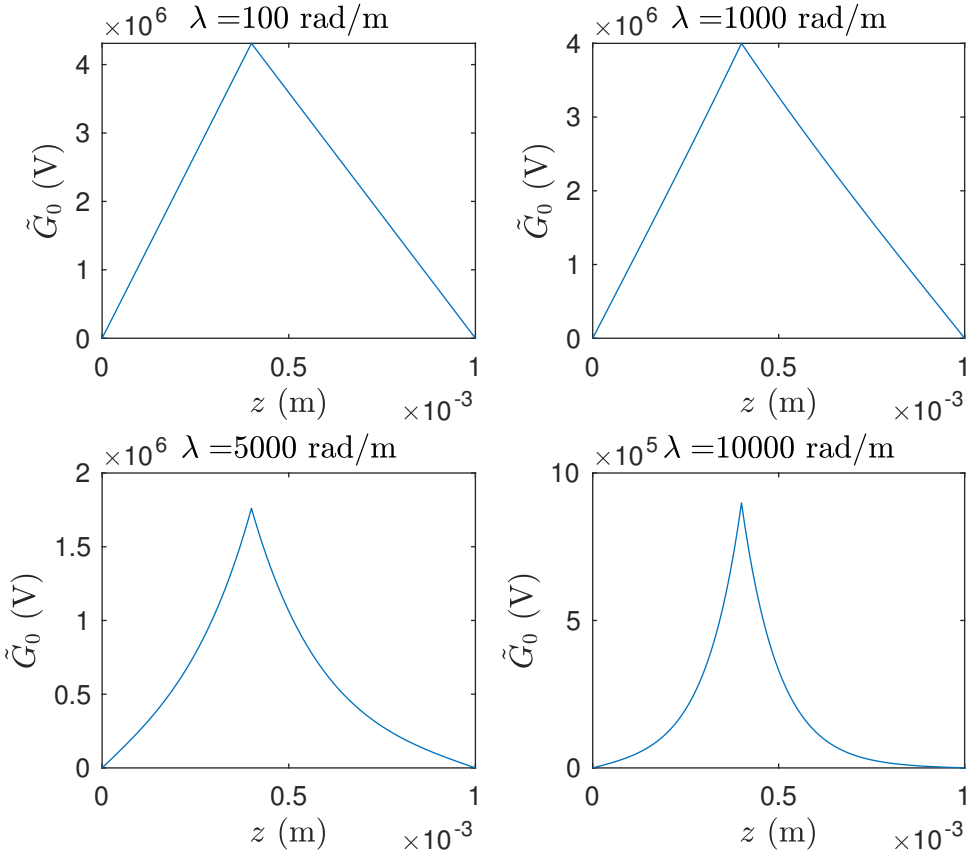

FIGURE 2.4: Spectral Domain Analytically Obtained Incident Green's Function $\tilde{G}_0$ Behavior

Chapter 3

Numerical Spectral Domain Scattered Potential Evaluation

Since we have the analytical expression for incident potential in the last chapter, we now solve for the scattered potential numerically, where the forward solver is a second order finite element method (FEM) based on Galerkin method. Once the numerical scattered potential is generated, we can recover the total potential by adding incident potential analytical result and the scattered potential.

3.1 ODE of Scattered Potential

Based on (1.22), at source location, $z = z'$, total potential and incident potential satisfy

$$\frac{d^2\tilde{G}}{dz^2} - \lambda^2\tilde{G} = -\frac{1}{2\pi\epsilon_{\text{src}}}\delta(z - z'), \tag{3.1}$$

and

$$\frac{d^2\tilde{G}_0}{dz^2} - \lambda^2\tilde{G}_0 = -\frac{1}{2\pi\epsilon_{\text{src}}}\delta(z - z'), \tag{3.2}$$

respectively. By subtracting (3.2) from (3.1), we have

$$\frac{d^2(\tilde{G} - \tilde{G}_0)}{dz^2} - \lambda^2(\tilde{G} - \tilde{G}_0) = 0. \tag{3.3}$$

The scattered potential, $\tilde{F} = \tilde{G} - \tilde{G}_0$, thus satisfies

$$\frac{d^2\tilde{F}}{dz^2} - \lambda^2\tilde{F} = 0. \tag{3.4}$$

At non-source locations, that is, when $z \neq z'$, the RHS's of ODE's for total potential and incident potential are both 0:

$$\frac{d^2\tilde{G}}{dz^2} - \lambda^2\tilde{G} = 0, \tag{3.5}$$

$$\frac{d^2\tilde{G}_0}{dz^2} - \lambda^2\tilde{G}_0 = 0. \tag{3.6}$$

Similarly, by subtracting (3.6) from (3.5), we have

$$\frac{d^2\tilde{F}}{dz^2} - \lambda^2\tilde{F} = 0. \tag{3.7}$$

In conclusion, for any z in $(0, d)$ except for dielectric interfaces, the ODE governing scattered potential is

$$\frac{d^2\tilde{F}}{dz^2} - \lambda^2\tilde{F} = 0. \tag{3.8}$$

Equation (3.8) does not hold at dielectric interfaces because the derivative of total potential does not exist at these locations, as illustrated in Figure 2.2.

3.2 Shape Functions

To approximate the spectral domain scattered potential with second order polynomials within each element, we discretize the z direction multilayer medium region $[0, d]$ into N_e elements in such a way that dielectric interfaces are at the edges of some elements. Elements are indexed sequentially from 1 to N_e starting from the bottom element to the top element. Each element is a second-order element containing three nodes. The bottom node, middle node and top node are named as $z_1^{(n)}$, $z_3^{(n)}$, and $z_2^{(n)}$ for nth element where $z_3^{(n)} = (z_1^{(n)} + z_2^{(n)})/2$. The medium discretization and a single example element are shown in Figure 3.1.

The shape functions used in second order FEM are [33]

$$S_1 = \frac{1}{2}\xi(\xi - 1), \qquad S_2 = \frac{1}{2}\xi(\xi + 1), \qquad S_3 = 1 - \xi^2, \tag{3.9}$$

where

$$\xi = \frac{2}{h}(z - z_3^{(n)}), \tag{3.10}$$

and h is the length of each element, meaning $h = z_2^{(n)} - z_1^{(n)}$. Shape functions of nth element are illustrated in Figure 3.2. The auxiliary variable ξ varies from $[-1, 1]$ as z moves from the bottom $z_1^{(n)}$ to top $z_2^{(n)}$ within nth element. At the three nodes $z_1^{(n)}, z_2^{(n)}$ and $z_3^{(n)}$, ξ is $-1, 1$, and 0 respectively, as shown in Figure 3.1. The derivatives of shape functions over z and ξ are listed as follows:

$$\frac{dS_1}{d\xi} = \xi - \frac{1}{2}, \qquad \frac{dS_1}{dz} = \frac{2}{h}(\frac{2}{h}(z - z_3^{(n)}) - \frac{1}{2}); \tag{3.11}$$

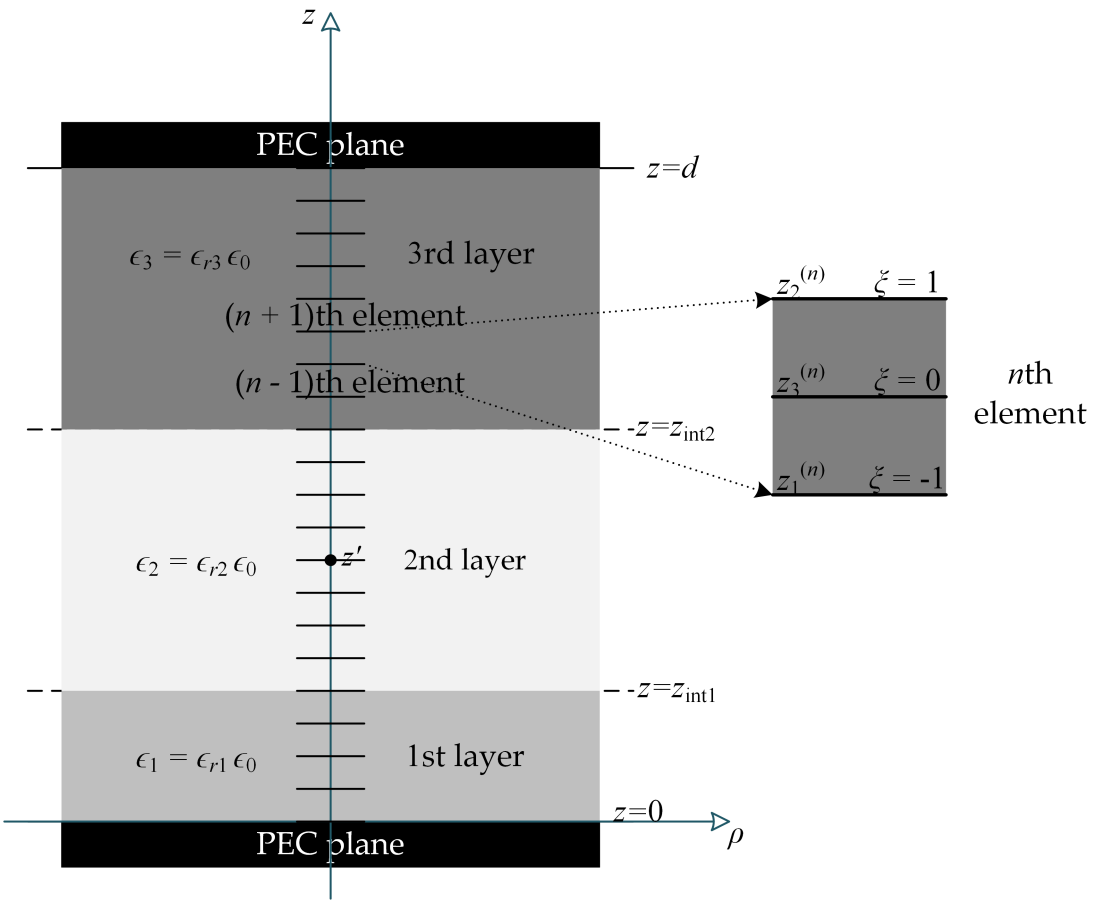

FIGURE 3.1: Discretization of Medium and Single Element Demonstration

$$\frac{dS_2}{d\xi} = \xi + \frac{1}{2}, \qquad \frac{dS_2}{dz} = \frac{2}{h}\left(\frac{2}{h}(z - z_3^{(n)}) + \frac{1}{2}\right); \tag{3.12}$$

$$\frac{dS_3}{d\xi} = -2\xi, \qquad \frac{dS_3}{dz} = -\frac{8}{h^2}(z - z_3^{(n)}). \tag{3.13}$$

So for any element n,

$$\left.\frac{dS_1}{dz}\right|_{z_1^{(n)}} = -\frac{3}{h}, \qquad \left.\frac{dS_1}{dz}\right|_{z_2^{(n)}} = \frac{1}{h}, \qquad \left.\frac{dS_1}{dz}\right|_{z_3^{(n)}} = -\frac{1}{h}; \tag{3.14}$$

$$\left.\frac{dS_2}{dz}\right|_{z_1^{(n)}} = -\frac{1}{h}, \qquad \left.\frac{dS_2}{dz}\right|_{z_2^{(n)}} = \frac{3}{h}, \qquad \left.\frac{dS_2}{dz}\right|_{z_3^{(n)}} = \frac{1}{h}; \tag{3.15}$$

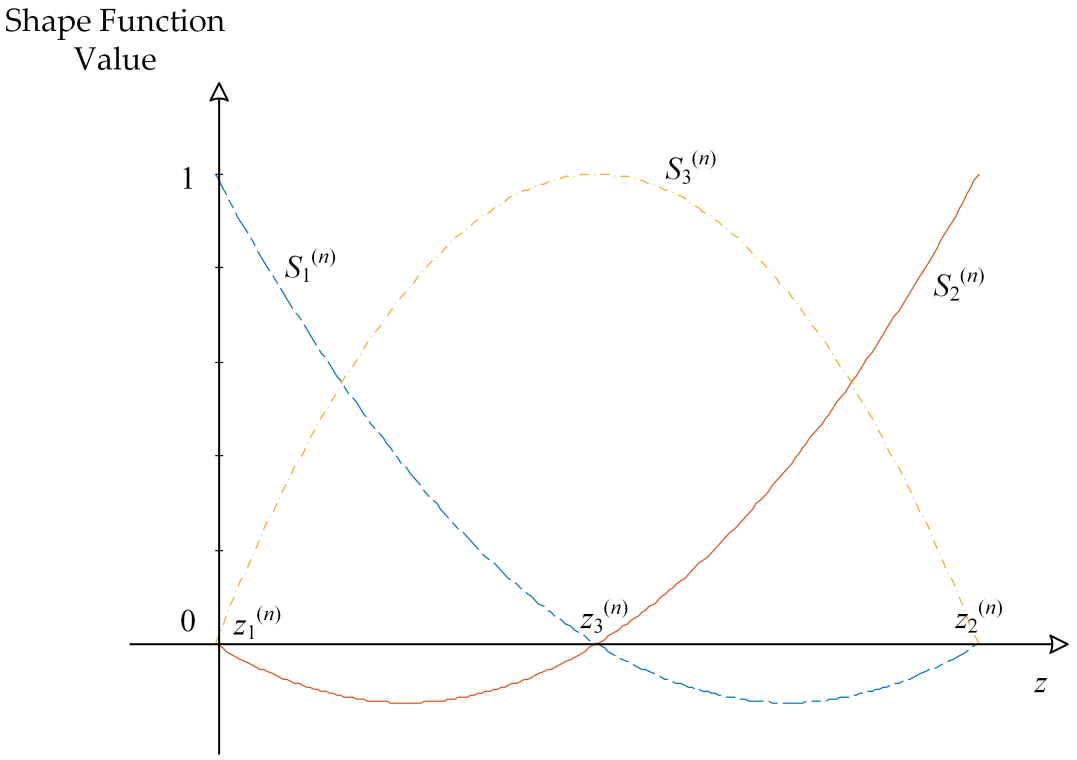

FIGURE 3.2: Shape Functions of An Arbitrary nth Element

$$\left.\frac{dS_3}{dz}\right|_{z_1^{(n)}} = \frac{4}{h}, \qquad \left.\frac{dS_3}{dz}\right|_{z_2^{(n)}} = -\frac{4}{h}, \qquad \left.\frac{dS_3}{dz}\right|_{z_3^{(n)}} = 0. \tag{3.16}$$

With the help of shape functions, scattered potential in nth element can be expressed as

$$\tilde{F}^{(n)} = \sum_{q=1}^{3} S_q(z)\tilde{f}_q^{(n)} \tag{3.17}$$

where $\tilde{f}_q^{(n)}$ is the local unknown scattered potential at the qth node of nth element. The derivative of the scattered potential is

$$\frac{d\tilde{F}^{(n)}}{dz} = \sum_{q=1}^{3} \tilde{f}_q^{(n)} \frac{dS_q(z)}{dz}. \tag{3.18}$$

3.3 Local and Global Weighted Residual

In the Galerkin method, the test function when evaluating weighted residual is the shape function itself [9], thus the local weighted residual for a single element n is

$$r_p^{(n)} = \int_{z_1^{(n)}}^{z_2^{(n)}} S_p^{(n)}(z) R dz, \qquad p = 1, 2, 3, \tag{3.19}$$

where R is the LHS of (3.8). Hence

$$r_p^{(n)} = \int_{z_1^{(n)}}^{z_2^{(n)}} S_p \frac{d^2\tilde{F}}{dz^2} dz - \lambda^2 \int_{z_1^{(n)}}^{z_2^{(n)}} S_p \tilde{F} dz \tag{3.20}$$

$$= -\int_{z_1^{(n)}}^{z_2^{(n)}} \frac{dS_p}{dz}\frac{d\tilde{F}}{dz} dz - \lambda^2 \int_{z_1^{(n)}}^{z_2^{(n)}} S_p \tilde{F} dz + \left(S_p \frac{d\tilde{F}}{dz} \right) \Bigg|_{z_1^{(n)}}^{z_2^{(n)}} \tag{3.21}$$

$$= -\sum_{q=1}^{3} \left(\int_{z_1^{(n)}}^{z_2^{(n)}} \frac{dS_p}{dz}\frac{dS_q}{dz} dz \right) \tilde{f}_q^{(n)} - \lambda^2 \sum_{q=1}^{3} \left(\int_{z_1^{(n)}}^{z_2^{(n)}} S_p S_q dz \right) \tilde{f}_q^{(n)} + \left(S_p \frac{d\tilde{F}}{dz} \right) \Bigg|_{z_1^{(n)}}^{z_2^{(n)}}, \qquad p = 1, 2, 3. \tag{3.22}$$

Align $r_p^{(n)}$ in a column vector for all $p = 1, 2, 3$, we have local residual vector $\mathbf{r}^{(n)}$ represented as

$$\mathbf{r}^{(n)} = \mathbf{A}^{(n)} \tilde{\mathbf{f}}^{(n)} + \mathbf{c}^{(n)}, \tag{3.23}$$

where $\mathbf{A}^{(n)} = \mathbf{A}_1^{(n)} + \lambda^2 \mathbf{A}_2^{(n)}$, and

$$A_{1_{p,q}}^{(n)} = -\int_{z_1^{(n)}}^{z_2^{(n)}} \frac{dS_p}{dz}\frac{dS_q}{dz} dz, \tag{3.24}$$

$$A_{2_{p,q}}^{(n)} = -\int_{z_1^{(n)}}^{z_2^{(n)}} S_p S_q dz. \tag{3.25}$$

The evaluations of (3.24), (3.25), and elements in vector $\mathbf{c}^{(n)}$ give

$$\mathbf{A}_1^{(n)} = \frac{1}{3h}\begin{bmatrix} -7 & -1 & 8 \\ -1 & -7 & 8 \\ 8 & 8 & -16 \end{bmatrix}, \tag{3.26}$$

$$\mathbf{A}_2^{(n)} = \frac{h}{15}\begin{bmatrix} -2 & \frac{1}{2} & -1 \\ \frac{1}{2} & -2 & -1 \\ -1 & -1 & -8 \end{bmatrix}, \tag{3.27}$$

$$\mathbf{c}^{(n)} = \begin{bmatrix} \left(S_1 \frac{d\tilde{F}}{dz}\right)\Big|_{z_1^{(n)}}^{z_2^{(n)}} \\ \left(S_2 \frac{d\tilde{F}}{dz}\right)\Big|_{z_1^{(n)}}^{z_2^{(n)}} \\ \left(S_3 \frac{d\tilde{F}}{dz}\right)\Big|_{z_1^{(n)}}^{z_2^{(n)}} \end{bmatrix} = \begin{bmatrix} -\frac{d\tilde{F}}{dz}\Big|_{z_1^{(n)}} \\ \frac{d\tilde{F}}{dz}\Big|_{z_2^{(n)}} \\ 0 \end{bmatrix}. \tag{3.28}$$

The global residual $\mathbf{r}$ is constructed by combining all contributions from local residuals $\mathbf{r}^{(n)}$ for all element n. The global residual can be written in

$$\mathbf{r} = \left(\mathbf{A}_1 + \lambda^2 \mathbf{A}_2\right)\tilde{\mathbf{F}} + \mathbf{c} \tag{3.29}$$

where $\tilde{\mathbf{F}}$ is the global unknown scattered potential vector. Set $\mathbf{r} = \mathbf{0}$, we have the system of linear equations (SLE)

$$\left(\mathbf{A}_1 + \lambda^2 \mathbf{A}_2\right)\tilde{\mathbf{F}} = -\mathbf{c}. \tag{3.30}$$

Matrices $\mathbf{A}_1$ and $\mathbf{A}_2$ have dimension $(2N_e{+}1){\times}(2N_e{+}1)$, $\mathbf{c} = [c_1, c_2, \cdots, c_{2N+1}]^T \in \mathbb{R}^{2N_e+1}$.

3.4 Boundary Conditions

We have three types of boundary conditions in the multilayer problem as explained when we sought analytical expression for spectral domain total potential in Section 2.2. How these boundary conditions are imposed when solving for scattered potential numerically is stated in the next three subsections.

3.4.1 PEC Planes

First of all, we consider scattered potential at top and bottom PEC planes. At these locations, $z = 0$ or $z = d$, $\tilde{F}\big|_{\text{PEC}} = (\tilde{G} - \tilde{G}_0)\big|_{\text{PEC}} = 0$ since $\tilde{G}$ and $\tilde{G}_0$ both vanish at PEC boundaries.

3.4.2 Continuity of Scattered Potential at Element Interfaces

The total potential $\tilde{G}$ and incident potential $\tilde{G}_0$ are both continuous at any location within the region of interest. So the scattered potential, as the difference between total potential and incident potential, is continuous as well. This continuity condition is implicitly imposed since the shape functions of two adjacent elements at their interface have the same value as 1. This property of shape functions is shown in Figure 3.3.

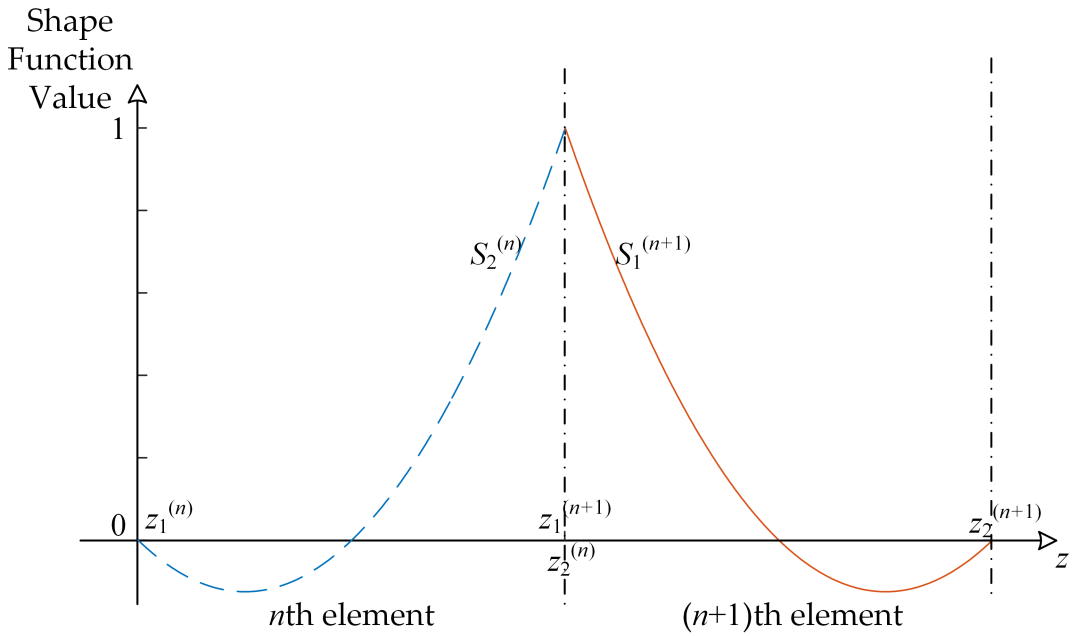

FIGURE 3.3: Shape Functions Having The Same Value As 1 Over Element Interfaces

3.4.3 Derivative of Scattered Potential

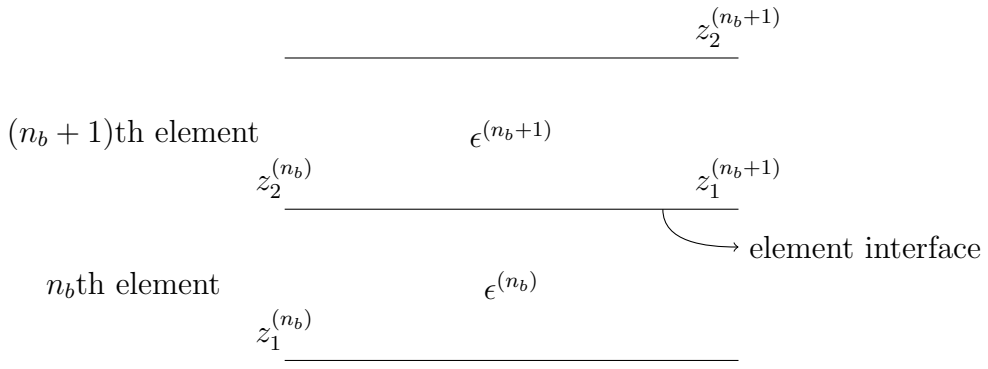

FIGURE 3.4: Interface Between Two Adjacent Elements

We examine the derivative of scattered potential at the interfaces between two adjacent elements. In the geometry shown in Figure 3.4, denote the index of element below element interface as n_b, such that the element above the element interface is element $(n_b + 1)$. We have two cases for this type of boundary:

3.4.3.1 Case 1: $\epsilon^{(n_b+1)} = \epsilon^{(n_b)}$

If $\epsilon^{(n_b+1)} = \epsilon^{(n_b)}$, the n_bth and (n_b+1)th elements are in the same medium layer. Then the normal component of electric flux density is continuous since no charge exists at the element interface:

$$(\mathbf{D}^{(n_b)}\big|_{\text{int}_{n_b,n_b+1}} - \mathbf{D}^{(n_b+1)}\big|_{\text{int}_{n_b,n_b+1}}) \cdot \mathbf{n}_{n_b,n_b+1} = \sigma_s = 0, \tag{3.31}$$

where $\mathbf{D}^{(n_b)}$ and $\mathbf{D}^{(n_b+1)}$ are electric flux density in the n_bth and (n_b+1)th element respectively. int_{n_b,n_b+1} represents the interface between n_bth and (n_b+1)th element. $\mathbf{n}_{n_b,n_b+1}$ is the normal vector pointing from n_bth element to (n_b+1)th element. Since we have Green's function representing the potential, the derivative of Green's function has a meaning of electric field. Then (3.31) can be written as

$$\epsilon^{(n_b+1)} \frac{d\tilde{G}}{dz}\bigg|_{z_1^{(n_b+1)}} = \epsilon^{(n_b)} \frac{d\tilde{G}}{dz}\bigg|_{z_1^{(n_b+1)}} = \epsilon^{(n_b)} \frac{d\tilde{G}}{dz}\bigg|_{z_2^{(n_b)}} \tag{3.32}$$

for the total potential and

$$\epsilon_{\text{src}} \frac{d\tilde{G}_0}{dz}\bigg|_{z_1^{(n_b+1)}} = \epsilon_{\text{src}} \frac{d\tilde{G}_0}{dz}\bigg|_{z_2^{(n_b)}} \tag{3.33}$$

for the incident potential. Equations (3.32) and (3.33) will lead to

$$\frac{d\tilde{F}}{dz}\bigg|_{z_1^{(n_b+1)}} = \frac{d\tilde{F}}{dz}\bigg|_{z_2^{(n_b)}}, \tag{3.34}$$

which reveals derivative of scattered potential must be continuous across the element interface under the assumption that $\epsilon^{(n_b+1)} = \epsilon^{(n_b)}$. When global vector $\mathbf{c}$ in (3.30) is constructed, equation (3.34) guarantees $c_{2n_b+1} = 0$ for each n_b if $\epsilon^{n_b+1} = \epsilon_b^n$.

3.4.3.2 Case 2: $\epsilon^{(n_b+1)} \neq \epsilon^{(n_b)}$

When element interface between n_bth and (n_b+1)th element is also a dielectric interface, that is, $\epsilon^{(n_b+1)} \neq \epsilon^{(n_b)}$, we have c_{2n_b+1} in global vector $\mathbf{c}$ being non-zero as

$$c_{2n_b+1} = \left.\frac{d\tilde{F}}{dz}\right|_{z_2^{(n_b)}} - \left.\frac{d\tilde{F}}{dz}\right|_{z_1^{(n_b+1)}} = \sum_{q=1}^{3} \tilde{f}_q^{(n_b)} \left(\left.\frac{dS_q}{dz}\right|_{z_2^{(n_b)}}\right) - \sum_{q=1}^{3} \tilde{f}_q^{(n_b+1)} \left(\left.\frac{dS_q}{dz}\right|_{z_1^{(n_b+1)}}\right) \tag{3.35}$$

$$= \frac{1}{h}\tilde{f}_1^{(n_b)} + \frac{3}{h}\tilde{f}_2^{(n_b)} - \frac{4}{h}\tilde{f}_3^{(n_b)} - \left(-\frac{3}{h}\tilde{f}_1^{(n_b+1)} - \frac{1}{h}\tilde{f}_2^{(n_b+1)} + \frac{4}{h}\tilde{f}_3^{(n_b+1)}\right) \tag{3.36}$$

$$= \frac{1}{h}\tilde{F}_{\text{int}-2} - \frac{4}{h}\tilde{F}_{\text{int}-1} + \frac{6}{h}\tilde{F}_{\text{int}} - \frac{4}{h}\tilde{F}_{\text{int}+1} + \frac{1}{h}\tilde{F}_{\text{int}+2}, \tag{3.37}$$

where $\tilde{F}_{int}$ is the unknown scattered potential at this dielectric interface in the global unknown vector. The constraint on normal electric flux density continuity of total potential does not change compared to the $\epsilon^{(n_b+1)} = \epsilon^{(n_b)}$ case, so

$$\epsilon^{(n_b+1)} \left.\frac{d\tilde{G}}{dz}\right|_{z_1^{(n_b+1)}} = \epsilon^{(n_b)} \left.\frac{d\tilde{G}}{dz}\right|_{z_2^{(n_b)}}. \tag{3.38}$$

Separating $\tilde{G}$ into $\tilde{F} + \tilde{G}_0$, we have

$$\epsilon^{(n_b+1)} \left.\frac{d\tilde{F}}{dz}\right|_{z_1^{(n_b+1)}} + \epsilon^{(n_b+1)} \left.\frac{d\tilde{G}_0}{dz}\right|_{z_1^{(n_b+1)}} = \epsilon^{(n_b)} \left.\frac{d\tilde{F}}{dz}\right|_{z_2^{(n_b)}} + \epsilon^{(n_b)} \left.\frac{d\tilde{G}_0}{dz}\right|_{z_2^{(n_b)}}. \tag{3.39}$$

Recall the derivative of scattered potential within an element represented in terms of shape functions as in (3.18), equation (3.39) then becomes

$$\epsilon^{(n_b+1)} \sum_{q=1}^{3} \tilde{f}_q^{(n_b+1)} \left(\left.\frac{dS_q}{dz}\right|_{z_1^{(n_b+1)}}\right) + \epsilon^{(n_b+1)} \left.\frac{d\tilde{G}_0}{dz}\right|_{z_1^{(n_b+1)}}$$
$$= \epsilon^{(n_b)} \sum_{q=1}^{3} \tilde{f}_q^{(n_b)} \left(\left.\frac{dS_q}{dz}\right|_{z_2^{(n_b)}}\right) + \epsilon^{(n_b)} \left.\frac{d\tilde{G}_0}{dz}\right|_{z_2^{(n_b)}}. \tag{3.40}$$

Simplifying (3.40) by moving $\tilde{F}_{\text{int}}$ to the LHS and all other terms to the RHS results in

$$\tilde{F}_{\text{int}} = \frac{1}{3\left(\epsilon^{(n_b+1)} + \epsilon^{(n_b)}\right)} \left(-\epsilon^{(n_b)} \tilde{F}_{int-2} + 4\epsilon^{(n_b)} \tilde{F}_{int-1} + 4\epsilon^{(n_b+1)} \tilde{F}_{int+1} - \epsilon^{(n_b+1)} \tilde{F}_{int+2} \right) + \frac{h\left(\epsilon^{(n_b+1)} - \epsilon^{(n_b)}\right)}{3\left(\epsilon^{(n_b+1)} + \epsilon^{(n_b)}\right)} \frac{d\tilde{G}_0}{dz} \Bigg|_{z_{\text{int}}} \tag{3.41}$$

Equation (3.41) contains the information on how the derivative of scattered potential jumps so that continuity of normal component of electric flux density is satisfied at the interface. To impose (3.41), we took two approaches that we call the weak form and strong form. They get their names on the criterion of whether (3.41) is rigorously imposed in SLE.

3.4.3.3 Weak Form

Plugging (3.41) into (3.37), we have

$$c_{2n_b+1} = \mathbf{C} \cdot \tilde{\mathbf{F}}_{\mathbf{nb}} + S_t, \tag{3.42}$$

where coefficient vector is

$$\mathbf{C} = \frac{\epsilon^{(n_b+1)} - \epsilon^{(n_b)}}{h\left(\epsilon^{(n_b+1)} + \epsilon^{(n_b)}\right)} \begin{bmatrix} 1 & -4 & 4 & -1 \end{bmatrix}, \tag{3.43}$$

Vector $\tilde{\mathbf{F}}_{\mathbf{nb}}$ contains neighbors of the dielectric interface unknown in global unknown vector

$$\tilde{\mathbf{F}}_{\mathbf{nb}} = \begin{bmatrix} \tilde{F}_{\text{int}-2} & \tilde{F}_{\text{int}-1} & \tilde{F}_{\text{int}+1} & \tilde{F}_{\text{int}+2} \end{bmatrix}^T. \tag{3.44}$$

The single term S_t is known value:

$$S_t = \frac{2\left(\epsilon^{(n_b+1)} - \epsilon^{(n_b)}\right)}{\epsilon^{(n_b+1)} + \epsilon^{(n_b)}} \frac{d\tilde{G}_0}{dz}\bigg|_{z_{\text{int}}}. \tag{3.45}$$

Plugging (3.42) into (3.30), $\mathbf{C}$ will be added to $\mathbf{A}_1$ in the $(2n_b+1)$th row in (3.30) after sign change. $-S_t$ will be a non-zero term in the RHS of (3.30). For each n_b satisfying $\epsilon^{(n_b+1)} \neq \epsilon^{(n_b)}$, that is, for each dielectric interface, we have one non-zero term in RHS of (3.30), and the $(2n_b+1)$th equation in the LHS of (3.30) altered.

Note, the process of modifying the $(2n_b+1)$th row of the original SLAE is not the sufficient and necessary condition to satisfying the $(2n_b+1)$th global residual being zero and (3.41) individually. The fact that (3.41) is not rigorously guaranteed gives this approach the name "weak form". This causes errors at the dielectric interfaces, and the error propagates over any location z.

Eventually we have a SLE as

$$(\mathbf{A} + \lambda^2 \mathbf{B})\tilde{\mathbf{F}} = \mathbf{b}. \tag{3.46}$$

Comparing (3.46) with (3.30), we know that $\mathbf{A_1}, \mathbf{A_2}$ are modified on the $(2n_b+1)$th rows once $\epsilon^{(n_b+1)} \neq \epsilon^{(n_b)}$ to give $\mathbf{A}$ and $\mathbf{B}$, RHS $\mathbf{b}$ has non-zero terms only at $(2n_b+1)$th rows. Matrices $\mathbf{A}$ and $\mathbf{B}$ have dimensions $(2N_e+1) \times (2N_e+1)$, $\mathbf{b} \in \mathbb{R}^{2N_e+1}$. The visualization of the SLE in a three layer medium is illustrated in Figure 3.5.

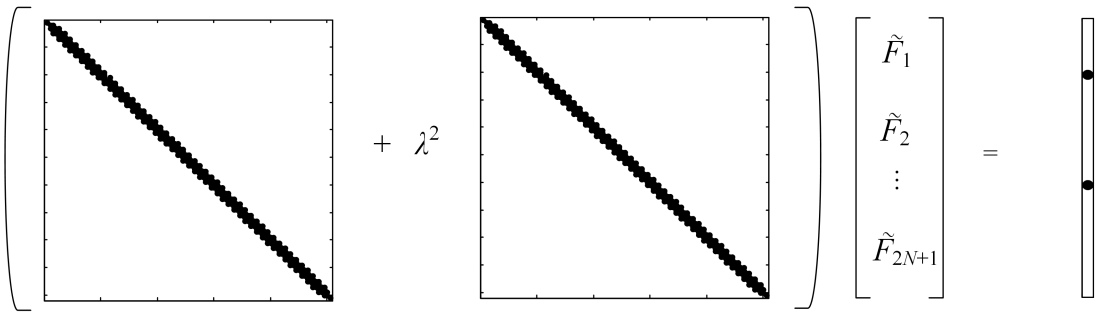

FIGURE 3.5: SLE Pattern for Weak Form

Notice non-zero values on the RHS occur at the indices of interface nodes. In scattered field formulation, the continuity of normal electric flux density indicates surface sources exist at dielectric interfaces. In comparison, when solving for total potential directly, the volumetric source occurs at the location of the point charge.

3.4.3.4 Strong Form

In the other approach named strong form, every dielectric interface unknown in the SLE (3.30) is replaced with its neighbors and known S_t as depicted in (3.41). That means the dielectric interface nodes unknowns are not involved in the SLE. Then N_{int} equations need to be removed to keep the SLE square where N_{int} is the total number of dielectric interfaces. The $(2n_b + 1)$th equations are removed from (3.30) for each n_b that lets $\epsilon^{(n_b+1)} \neq \epsilon^{(n_b)}$ hold, since they are on the rows in the SLE which correspond to the dielectric interface unknowns. Notice the elimination of these equations means the condition, $(2n_b + 1)$th global residual being zero, is removed for each eligible n_b. This shortage of these constraints introduces error. The final SLE from the strong form formulation is again in the form of

$$(\mathbf{A} + \lambda^2 \mathbf{B})\tilde{\mathbf{F}}_{\mathbf{nint}} = \mathbf{b}, \tag{3.47}$$

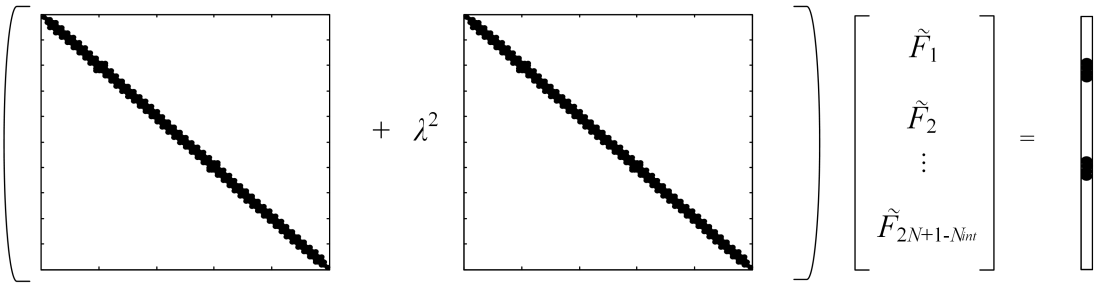

FIGURE 3.6: SLE Pattern for Strong Form

where $\mathbf{A}$ and $\mathbf{B}$ have dimensions $(2N_e + 1 - N_{\text{int}}) \times (2N_e + 1 - N_{\text{int}})$, $\tilde{\mathbf{F}}_{\mathbf{nint}} \in \mathbb{R}^{2N_e+1-N_{\text{int}}}$ is the unknown scattered potential vector excluding the dielectric interfaces nodes, $\mathbf{b} \in \mathbb{R}^{2N_e+1-N_{\text{int}}}$ as illustrated in Figure 3.6 for the same three-layer medium as in weak form.

After the SLE (3.47) is solved, we recover scattered potential at dielectric interfaces based on (3.41) and insert these values into $\tilde{\mathbf{F}}_{\mathbf{nint}}$ to have complete scattered potential list. The name of this approach "strong form" comes from the fact that (3.41) is guaranteed.

3.5 Numerical Results

The scattered field formulation is validated by multiple experiments on different medium specifications and different λ. Some results for the particular three-layer medium the same as in Section 2.2.2 are listed in this section.

When $\lambda = 5000\,\text{m}^{-1}\,\text{rad}$ and the number of total elements is 50 (so the number of total nodes is 101), the scattered potential obtained from different approaches are shown in Figure 3.7.

The analytical scattered potential is obtained by subtracting analytical incident potential introduced in Section 2.3 from analytical total potential introduced in Section 2.2. This analytical scattered potential is used as the standard to validate

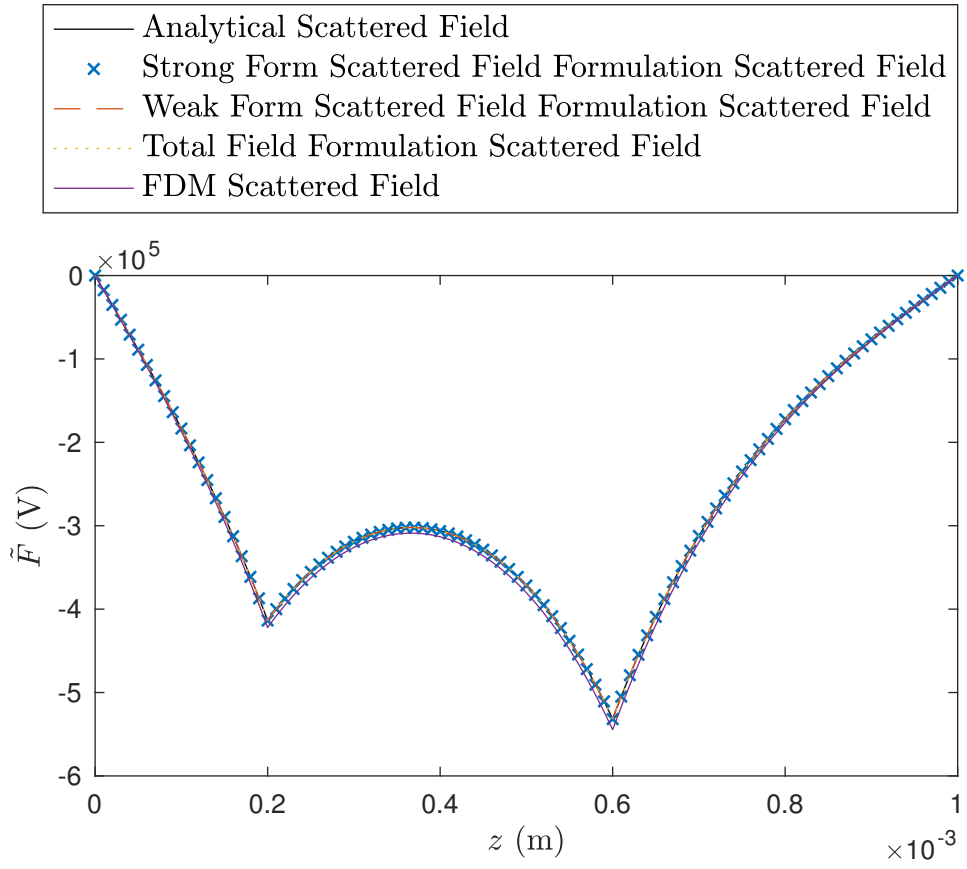

FIGURE 3.7: Scattered Potential $\tilde{F}(z, \lambda = 5000)$ from Different Methods

numerical results. By observation, finite difference method (FDM) gives the least accurate result. Although the aforementioned possible reasons leading to errors exist, the weak form and strong form second-order FEM return results with decent accuracies. The mean absolute percentage error (MAPE) for two methods are 0.0253% and 0.2287% respectively. Total field formulation refers to solving for total Green's function directly using second-order FEM solver.

The MAPE behavior as the number of total elements increases from 25, 50, 100, 200, 400 to 800 is shown in Figure 3.8 where both horizontal and vertical axes are in log scale. The error in either weak form or strong form scattered field formulation is of $\mathcal{O}(h^2)$ that matches second-order FEM error behavior expectation. However, the error in total field formulation behaves as quasi $\mathcal{O}(h^4)$ when second-order FEM

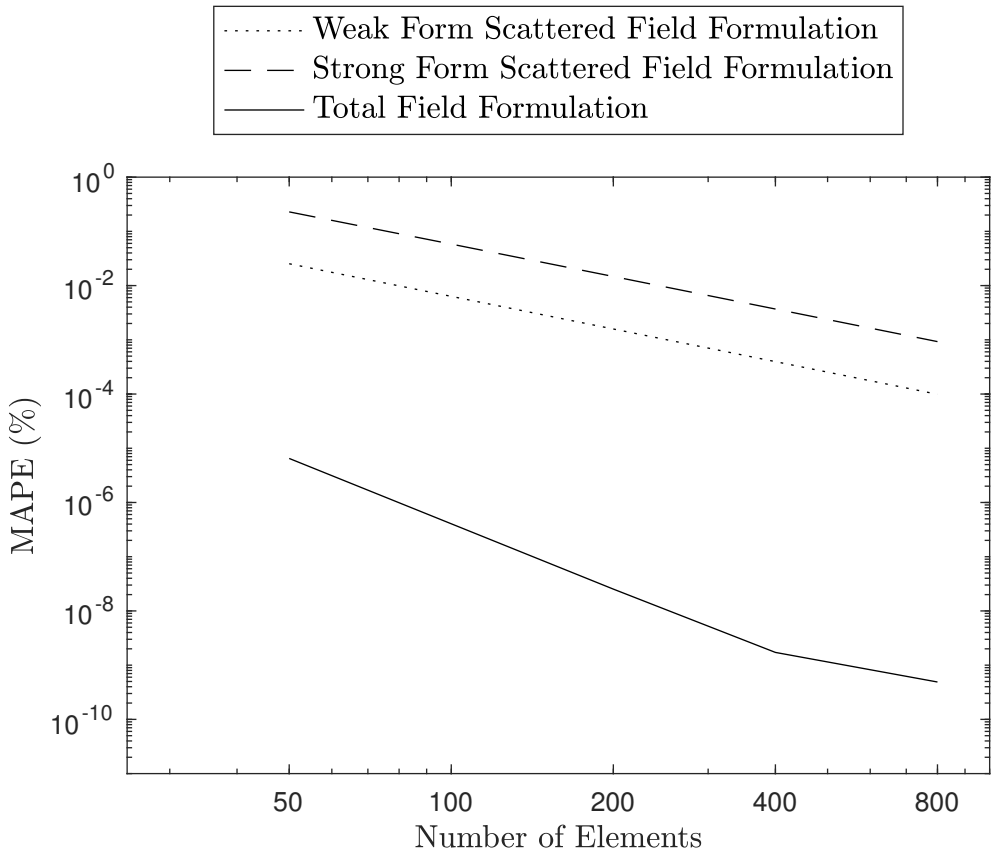

FIGURE 3.8: MAPE Behaviour

is used when the amount of elements is less than 400. This super convergence behavior will disappear as large number of elements are used.

The MAPE results reveal that scattered field formulation applied as weak form and strong form is error controllable as h refinement being performed but does not present better accuracy in the spectral domain. However, this may result due to the non-accurate imposition of boundary conditions. More work and investigation (imposing boundary conditions in a more careful way) need to be done to draw any further conclusion.

Since the weak form results seem to prevail over strong form in terms of accuracy as shown in Figure 3.8, it is adopted when constructing spectral domain total potential numerical result in order to convert the spectral domain total potential

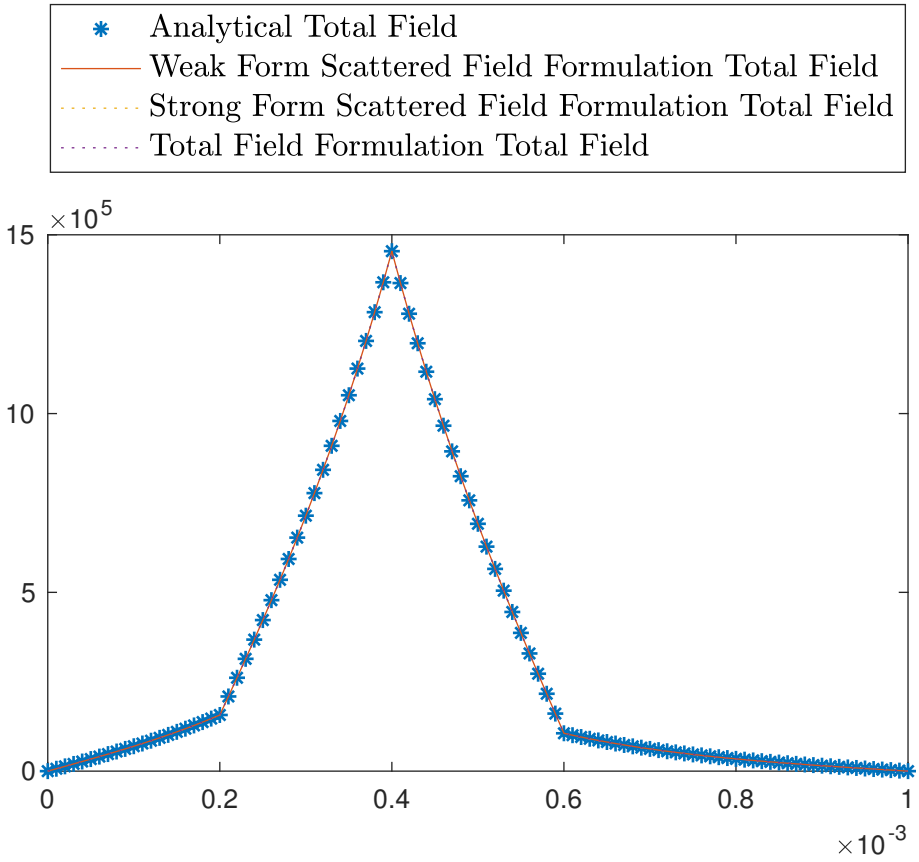

FIGURE 3.9: Total Potential $\tilde{G}(z, \lambda = 5000)$ from Different Methods

into the spatial domain in the next section. The total potential constructed from scattered potential and analytical incident potential using different method is given in Figure 3.9.

Chapter 4

Spatial domain Green's Function — Inverse Fourier-Bessel Transform of Its Spectral Domain Counterpart

4.1 Analytical Expressions for Spatial Domain Incident Potential

The spatial domain incident potential can be expressed in two forms analytically. The first one is derived from inverse Fourier-Bessel transform of spectral domain waveguide modes representation in Equation (2.34).

From [34] we know Bessel function of the first kind can be constructed by the average of Hankel functions of first and second kind:

$$J_0(\lambda\rho) = \frac{1}{2}\left(H_0^{(1)}(\lambda\rho) + H_0^{(2)}(\lambda\rho)\right). \tag{4.1}$$

Hankel functions of first and second kind can be mutually transmuted following relationship [34]

$$H_\nu^{(1)}(ze^{\pi i}) = -e^{-\nu\pi i}H_\nu^{(2)}(z). \tag{4.2}$$

Thus,

$$H_0^{(1)}(-z) = -H_0^{(2)}(z). \tag{4.3}$$

Let $a_n = n\pi/d$, then

$$\int_0^\infty \frac{1}{a_n^2+\lambda^2}J_0(\lambda\rho)\lambda d\lambda = \frac{1}{2}\left(\int_0^\infty \frac{H_0^{(1)}(\lambda\rho)}{a_n^2+\lambda^2}\lambda d\lambda + \int_0^\infty \frac{H_0^{(2)}(\lambda\rho)}{a_n^2+\lambda^2}\lambda d\lambda\right) \tag{4.4}$$

$$= \frac{1}{2}\left(\int_{-\infty}^0 \frac{-H_0^{(2)}(-\lambda\rho)}{a_n^2+\lambda^2}\lambda d\lambda + \int_0^\infty \frac{H_0^{(2)}(\lambda\rho)}{a_n^2+\lambda^2}\lambda d\lambda\right) = \frac{1}{2}\int_{-\infty}^\infty \frac{H_0^{(2)}(\lambda\rho)}{a_n^2+\lambda^2}\lambda d\lambda \tag{4.5}$$

$$= -\frac{\pi i}{2}H_0^{(2)}\left(-\frac{n\pi}{d}i\rho\right), \tag{4.6}$$

where i is the imaginary unit. Cauchy's residue theorem [35] is applied to simplify (4.5) to (4.6). Then we have spatial domain incident potential as inverse Fourier-Bessel transform of its spectral domain counterpart in the form of [32]

$$G_0 = \mathcal{FB}^{-1}\left\{\widetilde{G}_0\right\} = \frac{1}{\pi\epsilon_{\text{src}}d}\sum_{n=1}^\infty \sin\left(\frac{n\pi z}{d}\right)\sin\left(\frac{n\pi z'}{d}\right)\int_0^\infty \frac{J_0(\lambda\rho)\lambda}{\left(\frac{n\pi}{d}\right)^2+\lambda^2}d\lambda \tag{4.7}$$

$$= -\frac{i}{2\epsilon_{\text{src}}d}\sum_{n=1}^\infty \sin\left(\frac{n\pi z}{d}\right)\sin\left(\frac{n\pi z'}{d}\right)H_0^{(2)}\left(-i\frac{n\pi}{d}\rho\right). \tag{4.8}$$

The other analytical expression for incident potential is based on the method of images [28]. The location of images and their contributions to the potential are shown in Figure 4.1. The superscript represents where the potential contribution comes. The potential at (ρ, z) caused by a unit point charge at $(\rho' = 0, z')$ in a

homogeneous unbounded medium where permittivity being ϵ_{src} is

$$G_0^{\text{src}} = \frac{1}{4\pi\epsilon_{\text{src}}\sqrt{\rho^2 + (z - z')^2}} \tag{4.9}$$

in [28]. The images are produced by reflecting the original point charge and its images over two PEC planes. Define the list of odd indexed images is generated from the original point charge reflected by bottom PEC plane, top PEC plane, bottom PEC plane alternatively. The sign of charge needs to be flipped each time mirroring is performed in order to ensure the potentials at PEC planes are zero. For example, image one has a negative charge, being original point charge mirrored over bottom PEC plane; image three has a positive charge, it is a mirror image of image one over top PEC plane and so on. Similarly, images with even indices are the original point charge reflected by bottom PEC plane, top PEC plane, bottom PEC plane alternatively. The z coordinates, distances to the observation point and signs of charge of first seven images are listed in Table 4.1.

TABLE 4.1: Information of Point Charge's Images

	z Coordinate	$\lvert z_{\text{img}} - z' \rvert$	Sign of Charge
Img1	$-z'$	$\lvert z + z' \rvert$	-
Img2	$2d - z'$	$\lvert z + z' - 2d \rvert$	-
Img3	$2d + z'$	$\lvert z - z' - 2d \rvert$	+
Img4	$-(2d - z')$	$\lvert z - z' + 2d \rvert$	+
Img5	$-(2d + z')$	$\lvert z + z' + 2d \rvert$	-
Img6	$4d - z'$	$\lvert z + z' - 4d \rvert$	-
Img7	$4d + z'$	$\lvert z - z' - 4d \rvert$	+

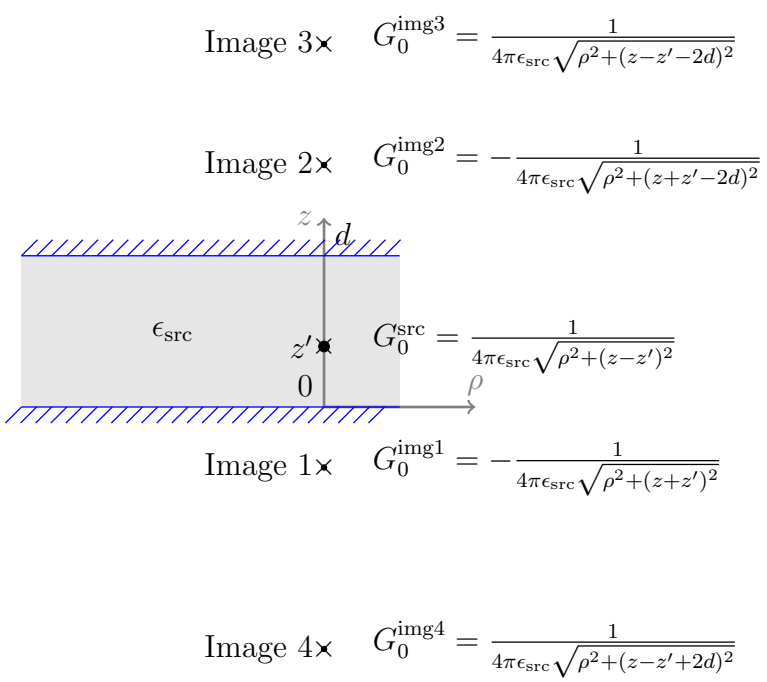

FIGURE 4.1: Images of Source in Multilayer Medium

.

Adding potential contributions from the original point charge source and all its images, we obtain the spatial incident potential as

$$\begin{aligned} G_0 = &\frac{1}{4\pi\epsilon_{\text{src}}\sqrt{\rho^2+(z-z')^2}} - \frac{1}{4\pi\epsilon_{\text{src}}\sqrt{\rho^2+(z+z')^2}} \\ &+ \sum_{n=1}^{\infty}\left(\frac{1}{4\pi\epsilon_{\text{src}}\sqrt{\rho^2+(z-z'+2nd)^2}} + \frac{1}{4\pi\epsilon_{\text{src}}\sqrt{\rho^2+(z-z'-2nd)^2}}\right. \\ &\left. - \frac{1}{4\pi\epsilon_{\text{src}}\sqrt{\rho^2+(z+z'+2nd)^2}} - \frac{1}{4\pi\epsilon_{\text{src}}\sqrt{\rho^2+(z+z'-2nd)^2}}\right) \end{aligned} \tag{4.10}$$

Expression (4.8) is more accurate in the far-source region since the Hankel functions captures the cylindrical behavior of the far potential, whereas (4.10) is more accurate as the near potential since the $1/\rho$ spherical wave like singularity is reserved.

4.2 Spectral Domain Scattered Potential in Pole Residual Form and Its Inverse Fourier-Bessel Transform to Spatial Domain

4.2.1 Spectral Domain Pole Residual Form Scattered Potential

As aforementioned, we only consider casting weak form in scattered field formulation to spatial domain. In order to do that, we first examine the pole residual form of the solution to SLE (3.46). Define the set $\{\mathbb{S}_{\text{int}}\}$ as the set of all interface nodes indices. The scattered Green's function vector is

$$\tilde{\mathbf{F}} = (\mathbf{A} + \lambda^2\mathbf{B})^{-1}\mathbf{b} = \mathbf{E}(\mathbf{D} + \lambda^2\mathbf{U})^{-1}\mathbf{T}\mathbf{b}, \tag{4.11}$$

where $\mathbf{T} = (\mathbf{BE})^{-1}$ and $\mathbf{EDE}^{-1} = \mathbf{B}^{-1}\mathbf{A}$ is the eigendecomposition of $\mathbf{B}^{-1}\mathbf{A}$. The scatted Green's function at ith node is consequently

$$\tilde{F}(\lambda, z_i; z') = \sum_{j' \in \mathbb{S}_{\text{int}}} b_{j'} \sum_{k=1}^{2N_e+1} \frac{E_{ik}T_{kj'}}{D_k + \lambda^2}. \tag{4.12}$$

The superscript prime on j means it is the dielectric interface node, where the surface source occurs. For simplicity, we first discuss two-layer medium case spatial domain scattered potential expression. Next, the result will be generalized to three or more layers cases. For medium with two dielectric layers, measure $|\{\mathbb{S}_{\text{int}}\}| = 1$, we have only one non-zero $b_{j'}$ that is written as

$$b_{j'} = -\frac{2(\epsilon_{i_l+1} - \epsilon_{i_l})}{\epsilon_{i_l+1} + \epsilon_{i_l}} \frac{d\tilde{G}_0}{dz}\bigg|_{z_{\text{int}}}, \tag{4.13}$$

where j' is the index of the only dielectric interface node in the discretization. Let's denote i_l as the index of layer beneath the dielectric interface that has j'th node on it. For example, in this two-layer case, j' corresponds to the first (and the only) interface, then $i_l = 1$ because the first layer is beneath the first dielectric interface following the convention in Figure 1.1. Evaluate the derivative of $\tilde{G}_0$ at the dielectric interface z_{int} based on (2.34), we have

$$\left.\frac{d\tilde{G}_0}{dz}\right|_{z_{\text{int}}} = \frac{1}{\epsilon_{\text{src}} d^2} \sum_{n=1}^{\infty} g(n) \frac{1}{a_n^2 + \lambda^2}, \tag{4.14}$$

where

$$g(n) = n \cos\left(\frac{n\pi z_{\text{int}}}{d}\right) \sin\left(\frac{n\pi z'}{d}\right). \tag{4.15}$$

So,

$$b_{j'} = -\frac{2(\epsilon_{i_l+1} - \epsilon_{i_l})}{(\epsilon_{i_l+1} + \epsilon_{i_l})\epsilon_{\text{src}} d^2} \sum_{n=1}^{\infty} g(n) \frac{1}{a_n^2 + \lambda^2}. \tag{4.16}$$

Once $b_{j'}$ is obtained, we have

$$\tilde{F}(\lambda, z_i; z_{j'}) = b_{j'} \sum_{k=1}^{2N_e+1} \frac{E_{ik} T_{kj'}}{D_k + \lambda^2} \tag{4.17}$$

$$= -\frac{2(\epsilon_{i_l+1} - \epsilon_{i_l})}{(\epsilon_{i_l+1} + \epsilon_{i_l})\epsilon_{\text{src}} d^2} \sum_{n=1}^{\infty} g(n) \left(\sum_{k=1}^{2N_e+1} \frac{E_{ik} T_{kj'}}{(D_k + \lambda^2)(a_n^2 + \lambda^2)} \right). \tag{4.18}$$

4.2.2 Spatial Domain Closed Form Scattered Potential

Spatial domain scattered potential is thus obtained by inverse Fourier-Bessel transform of spectral domain scattered potential as

$$F(\rho, z_i; z_{j'}) = \mathcal{F}\mathcal{B}^{-1}\{\tilde{F}(\lambda, z_i; z_{j'})\} = \int_0^{\infty} \tilde{F}(\lambda, z_i; z_{j'}) J_0(\lambda\rho) \lambda d\lambda \tag{4.19}$$

$$= -\frac{2(\epsilon_{i_l+1} - \epsilon_{i_l})}{(\epsilon_{i_l+1} + \epsilon_{i_l})\epsilon_{\text{src}} d^2} \sum_{n=1}^{\infty} g(n) \sum_{k=1}^{2N_e+1} E_{ik} T_{kj'} \int_0^{\infty} \frac{J_0(\lambda\rho)\lambda}{(D_k + \lambda^2)(a_n^2 + \lambda^2)} d\lambda. \tag{4.20}$$

The integral term in (4.20) is evaluated with the help of residue theorem as

$$\begin{aligned}
&\int_0^{\infty} \frac{J_0(\lambda\rho)\lambda}{(D_k + \lambda^2)(a_n^2 + \lambda^2)} d\lambda = \frac{1}{2} \int_{-\infty}^{\infty} \frac{H_0^{(2)}(\lambda\rho)\lambda}{(D_k + \lambda^2)(a_n^2 + \lambda^2)} d\lambda \\
&= \frac{-2\pi i}{2} \left(\text{Res}\left(\frac{H_0^{(2)}(\lambda\rho)\lambda}{(D_k + \lambda^2)(a_n^2 + \lambda^2)}, -i\sqrt{D_k} \right) + \text{Res}\left(\frac{H_0^{(2)}(\lambda\rho)\lambda}{(D_k + \lambda^2)(a_n^2 + \lambda^2)}, -ia_n \right) \right) \\
&= \frac{\pi i (H_0^{(2)}(-i\sqrt{D_k}\rho) - H_0^{(2)}(-ia_n\rho))}{2(D_k - a_n^2)}.
\end{aligned} \tag{4.21}$$

Bringing the result (4.21) back into (4.20), we have

$$F(\rho, z_i; z_{j'}) \tag{4.22}$$

$$= -\frac{2(\epsilon_{i_l+1} - \epsilon_{i_l})}{(\epsilon_{i_l+1} + \epsilon_{i_l})\epsilon_{\text{src}} d^2} \sum_{n=1}^{\infty} g(n) \sum_{k=1}^{2N_e+1} E_{ik} T_{kj'} \frac{\pi i (H_0^{(2)}(-i\sqrt{D_k}\rho) - H_0^{(2)}(-ia_n\rho))}{2(D_k - a_n^2)} \tag{4.23}$$

$$= c \sum_{n=1}^{\infty} g(n) \sum_{k=1}^{2N_e+1} E_{ik} T_{kj'} \frac{(H_0^{(2)}(-i\sqrt{D_k}\rho) - H_0^{(2)}(-ia_n\rho))}{D_k - a_n^2} = \tag{4.24}$$

$$c \left(\sum_{n=1}^{\infty} g(n) \sum_{k=1}^{2N_e+1} E_{ik} T_{kj'} \frac{H_0^{(2)}(-i\sqrt{D_k}\rho)}{D_k - a_n^2} - \sum_{n=1}^{\infty} g(n) \sum_{k=1}^{2N_e+1} E_{ik} T_{kj'} \frac{H_0^{(2)}(-ia_n\rho)}{D_k - a_n^2} \right) = \tag{4.25}$$

$$c \left(\sum_{k=1}^{2N_e+1} E_{ik} T_{kj'} H_0^{(2)}(-i\sqrt{D_k}\rho) \sum_{n=1}^{\infty} \frac{g(n)}{D_k - a_n^2} - \sum_{n=1}^{\infty} g(n) \sum_{k=1}^{2N_e+1} E_{ik} T_{kj'} \frac{H_0^{(2)}(-ia_n\rho)}{D_k - a_n^2} \right), \tag{4.26}$$

where the constant coefficient c is

$$c = -\frac{i(\epsilon_{i_l+1} - \epsilon_{i_l})\pi}{(\epsilon_{i_l+1} + \epsilon_{i_l})\epsilon_{\text{src}} d^2}. \tag{4.27}$$

The summation over n after the negative sign in (4.26) can be truncated (as

will be discussed later in Section 4.3) to avoid consuming large computational resource. But in the first summation part $\sum_{n=1}^{\infty} \frac{g(n)}{D_k - a_n^2}$ converges slowly because of its oscillating property. We use Poisson summation formula to find closed form for $\sum_{n=1}^{\infty} \frac{g(n)}{D_k - a_n^2}$ to speed up the calculation.

4.2.3 Applying Poisson Summation Formula on Oscillating Infinite Sum

Let's observe that

$$\sum_{n=1}^{\infty} \frac{g(n)}{D_k - a_n^2} = \frac{d}{\pi}\frac{d}{dz}\left(\sum_{n=1}^{\infty} \frac{\sin(a_n z)\sin(a_n z')}{D_k - a_n^2}\right)\Bigg|_{z_{\text{int}}}. \tag{4.28}$$

We examine $\sum_{n=1}^{\infty} \frac{\sin(a_n z)\sin(a_n z')}{D_k - a_n^2}$ first then take its derivative. Euler's formula gives

$$\sum_{n=1}^{\infty} \frac{\sin(a_n z)\sin(a_n z')}{D_k - a_n^2} \tag{4.29}$$

$$= -\frac{1}{4}\left(\sum_{n=1}^{\infty} \frac{e^{ia_n(z+z')}}{D_k - a_n^2} - \sum_{n=1}^{\infty} \frac{e^{ia_n(z-z')}}{D_k - a_n^2} - \sum_{n=1}^{\infty} \frac{e^{ia_n(z'-z)}}{D_k - a_n^2} + \sum_{n=1}^{\infty} \frac{e^{-ia_n(z+z')}}{D_k - a_n^2}\right) \tag{4.30}$$

$$= -\frac{1}{4}\left(\sum_{n=-\infty}^{\infty} \frac{e^{ia_n(z+z')}}{D_k - a_n^2} - \sum_{n=-\infty}^{\infty} \frac{e^{ia_n(z-z')}}{D_k - a_n^2}\right). \tag{4.31}$$

To use Poisson summation formula, we need to perform Fourier transform on

$$\frac{e^{ia_n(z+z')}}{D_k - a_n^2}, \tag{4.32}$$

and

$$\frac{e^{ia_n(z-z')}}{D_k - a_n^2}. \tag{4.33}$$

4.2.3.1 Fourier Transform of Equation (4.32)

Let $\pi(\frac{z+z'}{d} - 2k) = a$, $\frac{\pi}{d} = b$, $D^2 = \frac{D_k}{b^2}$, then

$$\mathcal{F}\left\{\frac{e^{ia_n(z+z')}}{D_k - a_n^2}\right\} = \int_{-\infty}^{\infty} \frac{e^{ia_n(z+z')}}{D_k - a_n^2} e^{-2\pi ink} dn = \int_{-\infty}^{\infty} \frac{e^{in\pi(\frac{z+z'}{d} - 2k)}}{D_k - (\frac{\pi}{d})^2 n^2} dn \tag{4.34}$$

$$= \frac{1}{b^2} \int_{-\infty}^{\infty} \frac{e^{ian}}{D^2 - n^2} dn = \frac{1}{b^2} \int_{-\infty}^{\infty} \frac{e^{ian}}{(D+n)(D-n)} dn. \tag{4.35}$$

Let's denote as D the primary branch of the square root of D_k/b^2. From the numerical results of the SLE, we know that $D_k \in \mathbb{R}^+$ or $D_k \in \mathbb{C}$. Thus, $D \in \mathbb{R}^+$ or $D \in \mathbb{C}$. For $D \in \mathbb{R}^+$,

$$\frac{1}{b^2} \int_{-\infty}^{\infty} \frac{e^{ian}}{(D+n)(D-n)} dn = -\frac{e^{iaD} - e^{-iaD}}{2b^2 D} \int_{-\infty}^{\infty} \frac{e^{iat}}{t} dt = \frac{e^{-iaD} - e^{iaD}}{2b^2 D} \pi i \operatorname{sgn}(a), \tag{4.36}$$

where

$$\operatorname{sgn}(a) = \begin{cases} 1, & k < \frac{z+z'}{2d} \\ -1, & k > \frac{z+z'}{2d} \end{cases}. \tag{4.37}$$

Since k is integer in the summation,

$$\operatorname{sgn}(a) = \begin{cases} 1, & k \leqslant 0 \\ -1, & k \geqslant 1 \end{cases}. \tag{4.38}$$

For $D \in \mathbb{C}$, D is either in the first or second quadrant, depending on the value of D_k. More specifically, when D_k is in the first quadrant, D is in the first quadrant as well. When D_k is in the fourth quadrant, D is in the second quadrant. The evaluation of the Fourier transform is not affected by the location of D as

$$\mathcal{F}\left\{\frac{e^{ia_n(z+z')}}{D_k - a_n^2}\right\} = \frac{1}{b^2} \int_{-\infty}^{\infty} \frac{e^{ian}}{(D+n)(D-n)} dn = -\frac{\pi i}{b^2 D} e^{iaD \operatorname{sgn}(a)}. \tag{4.39}$$

So based on Poisson summation formula, for $D_k \in \mathbb{R}^+$,

$$\sum_{n=-\infty}^{\infty} \frac{e^{ia_n(z+z')}}{D_k - a_n^2} = \sum_{k=-\infty}^{\infty} \mathcal{F}\left\{\frac{e^{ia_n(z+z')}}{D_k - a_n^2}\right\} = \sum_{k=-\infty}^{\infty} \frac{e^{-iaD} - e^{iaD}}{2b^2 D} \pi i \operatorname{sgn}(a) \tag{4.40}$$

$$= \frac{\pi i}{2b^2 D} \sum_{k=-\infty}^{0} \left(e^{-iaD} - e^{iaD}\right) - \frac{\pi i}{2b^2 D} \sum_{k=1}^{\infty} \left(e^{-iaD} - e^{iaD}\right) \tag{4.41}$$

$$= \frac{\pi i}{2b^2 D} \left(\left(\frac{e^{-i\pi(z+z')D/d}}{1 - e^{-i2\pi D}} - \frac{e^{i\pi(z+z')D/d}}{1 - e^{i2\pi D}} \right) - \left(\frac{e^{i\pi D(2-(z+z')/d)}}{1 - e^{i2\pi D}} - \frac{e^{i\pi D((z+z')/d-2)}}{1 - e^{-i2\pi D}} \right) \right) \tag{4.42}$$

$$= \frac{\pi i}{2b^2 D} \left(\frac{e^{-i\pi(z+z')D/d} + e^{i\pi D((z+z')/d-2)}}{1 - e^{-i2\pi D}} - \frac{e^{i\pi(z+z')D/d} + e^{i\pi D(2-(z+z')/d)}}{1 - e^{i2\pi D}} \right). \tag{4.43}$$

For $D \in \mathbb{C}$,

$$\sum_{n=-\infty}^{\infty} \frac{e^{ia_n(z+z')}}{D_k - a_n^2} = \sum_{k=-\infty}^{\infty} \mathcal{F}\left\{\frac{e^{ia_n(z+z')}}{D_k - a_n^2}\right\} = \sum_{k=-\infty}^{\infty} -\frac{\pi i}{b^2 D} e^{iaD \operatorname{sgn}(a)} \tag{4.44}$$

$$= -\frac{\pi i}{b^2 D} \left(\sum_{k=-\infty}^{0} e^{iaD} + \sum_{k=1}^{\infty} e^{-iaD} \right) \tag{4.45}$$

$$= -\frac{\pi i}{b^2 D} \left(\frac{e^{i\pi D(2-(z+z')/d)} + e^{i\pi(z+z')D/d}}{1 - e^{i2\pi D}} \right). \tag{4.46}$$

4.2.3.2 Fourier Transform of Equation (4.33)

For the Fourier transform in the second part of (4.31), the only difference between it and Fourier transform of the first part in (4.31) is a is changed to

$$\pi\left(\frac{z - z'}{d} - 2k\right). \tag{4.47}$$

This affects the result of $\operatorname{sgn}(a)$ with respect to integer k as

$$a > 0 \iff k < \frac{z - z'}{2d}. \tag{4.48}$$

If $z > z'$,

$$\operatorname{sgn}(a) = \begin{cases} 1 & k \leqslant 0 \\ -1 & k \geqslant 1 \end{cases}. \tag{4.49}$$

If $z < z'$,

$$\operatorname{sgn}(a) = \begin{cases} 1 & k \leqslant -1 \\ -1 & k \geqslant 0 \end{cases}. \tag{4.50}$$

However, the results of Fourier transform remain unchanged when $\operatorname{sgn}(a)$ is not explicitly expressed in terms of k. So for $D \in \mathbb{R}^+$,

$$\mathcal{F}\left\{\frac{e^{ia_n(z-z')}}{D_k - a_n^2}\right\} = \int_{-\infty}^{\infty} \frac{e^{ia_n(z-z')}}{D_k - a_n^2} e^{-i2\pi nk} dn = \frac{e^{-iaD} - e^{iaD}}{2b^2 D} \pi i \operatorname{sgn}(a). \tag{4.51}$$

For $D \in \mathbb{C}$,

$$\mathcal{F}\left\{\frac{e^{ia_n(z-z')}}{D_k - a_n^2}\right\} = -\frac{\pi i}{b^2 D} e^{iaD \operatorname{sgn}(a)}. \tag{4.52}$$

Let's apply Poisson summation formula in a similar manner, if $z > z'$, for real eigenvalue D_k,

$$\sum_{n=-\infty}^{\infty} \frac{e^{ia_n(z-z')}}{D_k - a_n^2} = \sum_{k=-\infty}^{\infty} \mathcal{F}\left\{\frac{e^{ia_n(z-z')}}{D_k - a_n^2}\right\} = \sum_{k=-\infty}^{\infty} \frac{e^{-iaD} - e^{iaD}}{2b^2 D} \pi i \operatorname{sgn}(a) \tag{4.53}$$

$$= \frac{\pi i}{2b^2 D} \sum_{k=-\infty}^{0} \left(e^{-iaD} - e^{iaD}\right) - \frac{\pi i}{2b^2 D} \sum_{k=1}^{\infty} \left(e^{-iaD} - e^{iaD}\right) \tag{4.54}$$

$$= \frac{\pi i}{2b^2 D} \left(\frac{e^{-i\pi(z-z')D/d} + e^{i\pi D((z-z')/d-2)}}{1 - e^{-i2\pi D}} - \frac{e^{i\pi(z-z')D/d} + e^{i\pi D(2-(z-z')/d)}}{1 - e^{i2\pi D}} \right). \tag{4.55}$$

For complex D_k we have

$$\sum_{n=-\infty}^{\infty} \frac{e^{ia_n(z-z')}}{D_k - a_n^2} = \sum_{k=-\infty}^{\infty} \mathcal{F}\left\{\frac{e^{ia_n(z-z')}}{D_k - a_n^2}\right\} = \sum_{k=-\infty}^{\infty} -\frac{\pi i}{b^2 D} e^{iaD\,\mathrm{sgn}(a)} \tag{4.56}$$

$$= -\frac{\pi i}{b^2 D}\left(\sum_{k=-\infty}^{0} e^{iaD} + \sum_{k=1}^{\infty} e^{-iaD}\right) \tag{4.57}$$

$$= -\frac{\pi i}{b^2 D}\left(\frac{e^{i\pi(z-z')D/d} + e^{i\pi D(2-(z-z')/d)}}{1 - e^{i2\pi D}}\right). \tag{4.58}$$

If $z < z'$, for real D_k,

$$\sum_{n=-\infty}^{\infty} \frac{e^{ia_n(z-z')}}{D_k - a_n^2} = \sum_{k=-\infty}^{\infty} \mathcal{F}\left\{\frac{e^{ia_n(z-z')}}{D_k - a_n^2}\right\} = \sum_{k=-\infty}^{\infty} \frac{e^{-iaD} - e^{iaD}}{2b^2 D} \pi i\,\mathrm{sgn}(a) \tag{4.59}$$

$$= \frac{\pi i}{2b^2 D}\sum_{k=-\infty}^{-1}\left(e^{-iaD} - e^{iaD}\right) - \frac{\pi i}{2b^2 D}\sum_{k=0}^{\infty}\left(e^{-iaD} - e^{iaD}\right) \tag{4.60}$$

$$= \frac{\pi i}{2b^2 D}\left(\left(\frac{e^{-i\pi D(2+(z-z')/d)}}{1 - e^{-i2\pi D}} - \frac{e^{i\pi D(2+(z-z')/d)}}{1 - e^{i2\pi D}}\right) - \left(\frac{e^{-i\pi D(z-z')/d}}{1 - e^{i2\pi D}} - \frac{e^{i\pi D(z-z')/d}}{1 - e^{-i2\pi D}}\right)\right) \tag{4.61}$$

$$= \frac{\pi i}{2b^2 D}\left(\frac{e^{-i\pi D(2+(z-z')/d)} + e^{i\pi D(z-z')/d}}{1 - e^{-i2\pi D}} - \frac{e^{i\pi D(2+(z-z')/d)} + e^{-i\pi D(z-z')/d}}{1 - e^{i2\pi D}}\right). \tag{4.62}$$

For complex D_k we have

$$\sum_{n=-\infty}^{\infty} \frac{e^{ia_n(z-z')}}{D_k - a_n^2} = \sum_{k=-\infty}^{\infty} \mathcal{F}\left\{\frac{e^{ia_n(z-z')}}{D_k - a_n^2}\right\} = \sum_{k=-\infty}^{\infty} -\frac{\pi i}{b^2 D} e^{iaD\,\mathrm{sgn}(a)} \tag{4.63}$$

$$= -\frac{\pi i}{b^2 D}\left(\sum_{k=-\infty}^{-1} e^{iaD} + \sum_{k=0}^{\infty} e^{-iaD}\right) \tag{4.64}$$

$$= -\frac{\pi i}{b^2 D}\left(\frac{e^{i\pi D(2+(z-z')/d)} + e^{-i\pi D(z-z')/d}}{1 - e^{i2\pi D}}\right). \tag{4.65}$$

4.2.3.3 Final Spatial Domain Closed Form Scattered Potential

After some manipulations, based on Poisson summation formula, for real D_k, we get

$$\sum_{n=1}^{\infty} \frac{g(n)}{D_k - a_n^2} = \frac{d}{\pi}\frac{d}{dz}\left(\sum_{n=1}^{\infty} \frac{\sin(a_n z)\sin(a_n z')}{D_k - a_n^2}\right)\Bigg|_{z_{\text{int}}} \tag{4.66}$$

$$= -\frac{d}{4\pi}\left(\frac{d}{dz}\left(\sum_{n=-\infty}^{\infty} \frac{e^{ia_n(z+z')}}{D_k - a_n^2}\right)\Bigg|_{z_{\text{int}}} - \frac{d}{dz}\left(\sum_{n=-\infty}^{\infty} \frac{e^{ia_n(z-z')}}{D_k - a_n^2}\right)\Bigg|_{z_{\text{int}}}\right) \tag{4.67}$$

$$= \begin{cases} \dfrac{d^2}{8\pi}\Bigg(\dfrac{e^{-i\pi D(z_{\text{int}}-z')/d} + e^{i\pi D((z_{\text{int}}+z')/d-2)}}{1-e^{-i2\pi D}} \\ \quad - \dfrac{e^{-i\pi D(z_{\text{int}}+z')/d} + e^{i\pi D((z_{\text{int}}-z')/d-2)}}{1-e^{-i2\pi D}} \\ \quad + \dfrac{e^{i\pi D(z_{\text{int}}-z')/d} + e^{-i\pi D((z_{\text{int}}+z')/d-2)}}{1-e^{i2\pi D}} \\ \quad - \dfrac{e^{i\pi D(z_{\text{int}}+z')/d} + e^{-i\pi D((z_{\text{int}}-z')/d-2)}}{1-e^{i2\pi D}}\Bigg), & \text{if } z_{\text{int}} > z' \\ \dfrac{d^2}{8\pi}\Bigg(\dfrac{e^{-i\pi D((z_{\text{int}}-z')d+2)} + e^{i\pi D((z_{\text{int}}+z')/d-2)}}{1-e^{-i2\pi D}} \\ \quad - \dfrac{e^{-i\pi D(z_{\text{int}}+z')/d} + e^{i\pi D(z_{\text{int}}-z')/d}}{1-e^{-i2\pi D}} \\ \quad + \dfrac{e^{i\pi D((z_{\text{int}}-z')/d+2)} + e^{-i\pi D((z_{\text{int}}+z')/d-2)}}{1-e^{i2\pi D}}, & \text{if } z_{\text{int}} < z' \\ \quad - \dfrac{e^{i\pi D(z_{\text{int}}+z')/d} + e^{-i\pi D(z_{\text{int}}-z')/d}}{1-e^{i2\pi D}}\Bigg) \end{cases}. \tag{4.68}$$

Similarly, for complex D_k, we get

$$\sum_{n=1}^{\infty} \frac{g(n)}{D_k - a_n^2}$$

$$= -\frac{d}{4\pi}\left(\frac{d}{dz}\left(\sum_{n=-\infty}^{\infty} \frac{e^{ia_n(z+z')}}{D_k - a_n^2}\right)\Bigg|_{z_{\text{int}}} - \frac{d}{dz}\left(\sum_{n=-\infty}^{\infty} \frac{e^{ia_n(z-z')}}{D_k - a_n^2}\right)\Bigg|_{z_{\text{int}}}\right) \tag{4.69}$$

$$= \begin{cases} \dfrac{d^2}{4\pi}\cdot\Bigg(\dfrac{e^{-i\pi D(2-(z_{\text{int}}+z')/d)} - e^{-i\pi D(z_{\text{int}}+z')/d}}{1-e^{-i2\pi D}} \\ \quad + \dfrac{e^{-i\pi D(z_{\text{int}}-z')/d} - e^{-i\pi D(2-(z_{\text{int}}-z')/d)}}{1-e^{-i2\pi D}}\Bigg), & \text{if } z_{\text{int}} > z' \\ \dfrac{d^2}{4\pi}\cdot\Bigg(\dfrac{-e^{-i\pi D(z_{\text{int}}+z')/d} + e^{-i\pi D(2-(z_{\text{int}}+z')/d)}}{1-e^{-i2\pi D}} \\ \quad + \dfrac{e^{-i\pi D(2+(z_{\text{int}}-z')/d)} - e^{i\pi D(z_{\text{int}}-z')/d}}{1-e^{-i2\pi D}}\Bigg), & \text{if } z_{\text{int}} < z' \end{cases}. \tag{4.70}$$

Based on the comparison on z_{int} and z', define results in (4.68) or (4.70) as a function $\kappa_k(z_{\text{int}}, z', d)$ which is solely dependent on medium geometry. Plugging $\kappa_k(z_{\text{int}}, z', d)$ back into (4.26), we have the spatial domain solution in closed form with accuracy controllable to machine precision, if needed:

$$F(\rho, z_i; z_{j'}) = c \left(\sum_{k=1}^{2N_e+1} E_{ik} T_{kj} H_0^{(2)}(-i\sqrt{D_k}\rho) \kappa_k(z_{\text{int}}, z', d) - \sum_{n=1}^{\infty} g(n) \sum_{k=1}^{2N_e+1} E_{ik} T_{kj'} \frac{H_0^{(2)}(-ia_n\rho)}{D_k - a_n^2} \right). \tag{4.71}$$

Equation (4.71) gives two-layer medium scattered Green's function expression. For three or more layers case, the scattered potential will be

$$F(\rho, z_i; z_{j'}) = \sum_{j' \in \mathbb{S}_{\text{int}}} c_{j'} \left(\sum_{k=1}^{2N_e+1} E_{ik} T_{kj} H_0^{(2)}(-i\sqrt{D_k}\rho) \kappa_k(z_{j'}, z', d) - \sum_{n=1}^{\infty} g(n) \sum_{k=1}^{2N_e+1} E_{ik} T_{kj'} \frac{H_0^{(2)}(-ia_n\rho)}{D_k - a_n^2} \right), \tag{4.72}$$

where c'_j is the coefficient relating to each interface, calculated according to (4.27).

4.3 Truncation of Summation in Spatial Domain Scattered Potential Expression

Comparing (4.71) with the total Green's function result in [29], we know for two-layer case, the first summation term in (4.71) is analogous with the closed-form expression for the total potential in [29]. Therefore, the computational cost for their evaluation is similar. The second summation term in (4.71), however, involves the infinite series over n. We have to truncate the summation series in (4.71) to enable its numerical evaluation. For large arguments, Hankel functions behave like

exponentials [8]

$$H_0^{(2)}(z) \sim \sqrt{\frac{2}{\pi z}} e^{-i(z-\frac{\pi}{4})}. \tag{4.73}$$

Consider the Hankel function in the summation after negative sign in (4.71) which has $-ia_n\rho$ as argument, as n tends to ∞,

$$H_0^{(2)}(-ia_n\rho) \sim \sqrt{\frac{2i}{\pi a_n \rho}} e^{-a_n\rho} e^{i\frac{\pi}{4}}. \tag{4.74}$$

For a given ρ and tolerance TOL, define

$$N = \left\lceil -\frac{d \ln \text{TOL}}{\rho\pi} \right\rceil, \tag{4.75}$$

then $\forall n > N$, $H_0^{(2)}(-ia_n\rho) < \text{TOL}$ and, thus, this Hankel function contribution into the series can be omitted. In this way the summation over n from 1 to ∞ in (4.71) can be truncated to run from 1 to N.

Getting the series over the Hankel functions $H_0^{(2)}(-i\sqrt{D_k}\rho)$ in (4.71), is not as critical since it is bounded by $2N_e + 1$. However, in the interest of reducing computational effort, it is advisable to perform truncation of this summation, when ρ is not overly small. Some eigenvalues D_k have large magnitude, hence, when ρ is not small, the exponential attenuation of the Hankel function

$$H_0^{(2)}(-i\sqrt{D_k}\rho) \sim \sqrt{\frac{2i}{\pi\sqrt{D_k}\rho}} e^{-\sqrt{D_k}\rho} e^{i\frac{\pi}{4}}. \tag{4.76}$$

allows for omission of the terms, which have contribution below desired tolerance level [24]. To elaborate, let's consider the case $D_k \in \mathbb{R}^+$ and arrange all D_k in an increasing manner. Then, for any

$$D_k > \left(\frac{\ln \text{TOL}}{\rho} \right)^2, \tag{4.77}$$

series terms containing $H_0^{(2)}(-i\sqrt{D_k}\rho)$ are below tolerance (TOL) and can be omitted. Similarly, if $D_k \in \mathbb{C}$,

$$e^{-\sqrt{D_k}\rho} = e^{-\sqrt{|D_k|}\cos\left(\frac{\theta}{2}\right)\rho}, \tag{4.78}$$

where θ is the phase of D_k. For any

$$|D_k| > \left(\frac{\ln \mathrm{TOL}}{\rho \cos\left(\frac{\theta}{2}\right)}\right)^2, \tag{4.79}$$

$H_0^{(2)}(-i\sqrt{D_k}\rho)$ is smaller than TOL and the series terms involving it can be omitted.

4.4 Numerical Results

For the medium specification in Figure 2.1, the near potential (which is Green's function at an observation point near the point charge) and the far potential are tested to validate the new method. Results are shown in the next two subsections. The experiments are carried out when number of total elements is 50. Length between two adjacent nodes is 0.01 mm.

4.4.1 Near Potential

To test the near potential results, we take the observation point $z = z' = 0.4\,\mathrm{mm}$. The radial distance ρ is tested from 1 µm to 1 mm. Total number of elements is fixed as 50 to avoid too extensive computational cost when spatial domain standard is obtained. Spatial domain standard is obtained by numerically integrating the spectral domain analytical expression for total Green's function. The spatial

Green's function's behaviour as ρ increases is shown in Figure 4.2. Both horizontal and vertical axes are in log scale.

The black dotted line depicts the incident potential. All other lines are total Green's function evaluated using different methods. As we anticipated, near the source the incident potential has $1/\rho$ singularity. This $1/\rho$ singularity is stronger than the $\log(\rho)$ singularity that Hankel function preserves when input argument is small [8]. This fact makes incident potential dominate the near potential so much that scattered potential contribution can be neglected. In this case, if the incident potential is accurately calculated, we can have an overall accurate total Green's function. Since the scattered field formulation keeps the accurate analytical incident potential, it provides accurate total Green's function result near the source. However, in the traditional method (referred to as total potential formulaion) that solves total potential directly as in [29], total Green's function is represented in terms of superposition of Hankel functions, which can not grasp the singularity of incident potential as $1/\rho$ in (4.10) and produces high error.

4.4.2 Far Potential

When the observation point is far from the source, both the incident and scattered potentials may be significantly contributing into the total potential. Hence, both the incident and the scattered potential contributions must be accurately calculated. When observation point is fixed at $z = 0.8\,\text{mm}$ and ρ varies from $0.1\,\text{mm}$ to $4\,\text{mm}$, the total Green's functions computed by different methods are illustrated in Figure 4.3. In the far region, Green's function behaves like cylindrical wave and thus can be recovered by Hankel functions as in the total potential method. However, Green's function calculated from total field formulation is still less accurate than that obtained from the scattered field formulation.

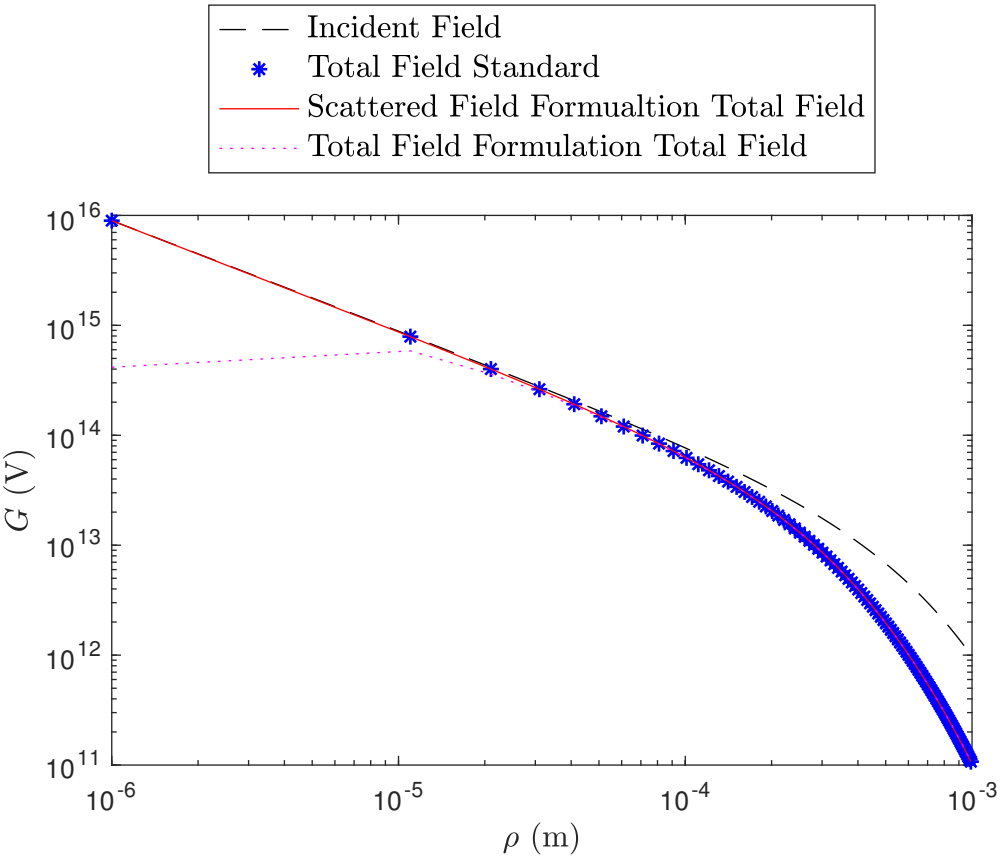

FIGURE 4.2: Spatial Green's Function $G(z = 0.4\,\text{mm},\, z' = 0.4\,\text{mm},\, \rho)$

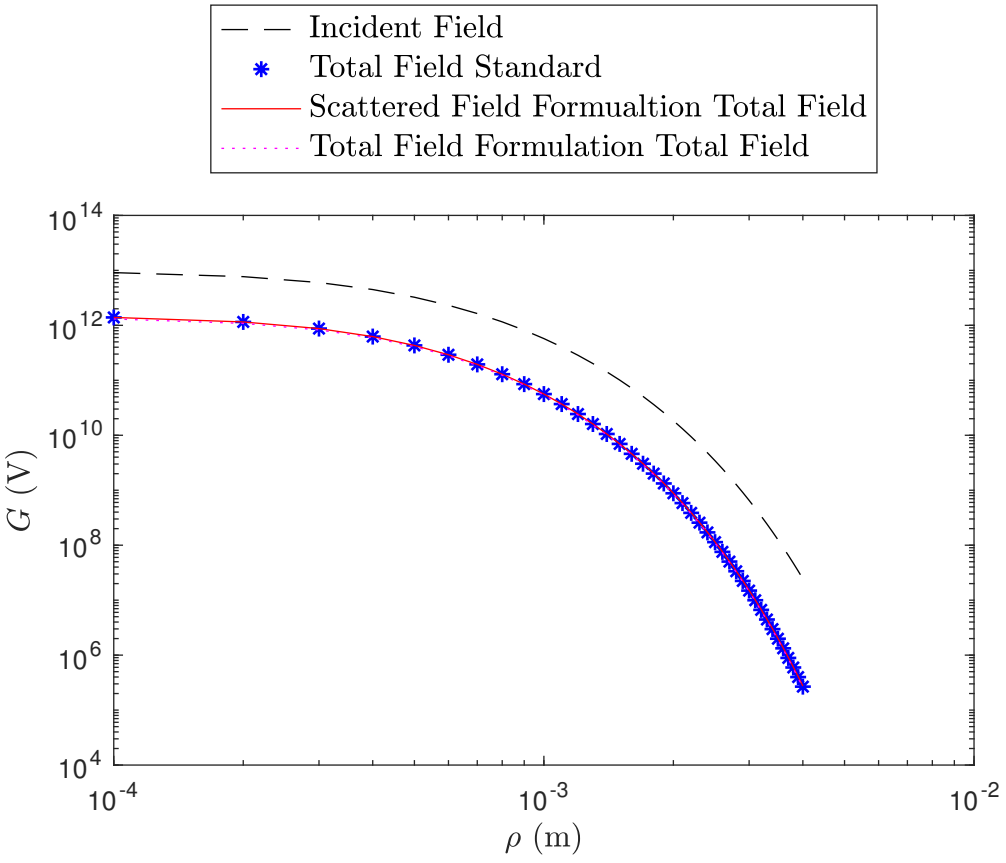

FIGURE 4.3: Spatial Green's Function $G(z = 0.8\,\text{mm},\, z' = 0.4\,\text{mm},\, \rho)$

Chapter 5

Summary and Future Work

In this work, a new method for uniformly accurate computation of layered medium Green's functions is proposed. The proof of concept for the new method is demonstrated on the example of electrostatic Green's function of multilayered medium bounded by PEC planes. The method is called "the scattered field formulation of the Spectral Differential Equation Approximation Method" or, simply, *scattered field SDEAM*. The method provides high accuracy of Green's function approximation in both near and far field and maintains comparable computational cost to that of the traditional total potential formulation of SDEAM, which fails to approximate the near field accurately. The uniform high accuracy of the approximation is achieved by preserving incident potential, which dominates the total Green's function in the near zone, in its analytical form, while numerically approximating only the scattered field. The FEM solution of the ordinary differential equation governing the spectrum of the scattered field Green's function is used. Such FEM solver provides error controllable evaluation of the Green's function in the spectral domain. There are different ways of incorporating the boundary conditions into the ODE governing the spectrum of the scattered field though, which result in "weak" and "strong" forms of electric flux continuity enforcement. These two approaches intrinsically introduce the error into the approximation of

the scattered field Green's function. However, they do it in different ways. Despite the error introduced into the spectral domain scattered field by the enforcement of the boundary conditions, the spatial domain result, which is of interest, exhibits better accuracy than the total field formulation, especially when the observation is near the source. So, the results in this work show that the new method of solving for the scattered potential numerically, while introducing the analytical form of the incident potential, can be beneficial in terms of accuracy. This new method promises to produce even higher accuracy, if the boundary condition at the interfaces of the layers are enforced more accurately. Studies of alternative methods for enforcement of the boundary conditions in the proposed scattered field formulation of SDEAM will be a subject of future work.

Preliminary studies have shown that alternative solution techniques such as Discontinuous Galerkin Method (DGM) can allow for a more straightforward approach to integrating boundary conditions into the ODE and, hence, produce a better accuracy than FEM applied in this work, when the same number of elements is taken in both methods. The use of DGM in the proposed scattered field formulation of the SDEAM will be studied further. It is also expected to shed light on how to enforce the boundary conditions in the FEM solution more accurately. In the future work, the scattered potential formulation of SDEAM will be generalized to cases of full-wave Green's function formulations in both the traditional vector potential case and Michalski-Zheng's mixed potential case.

Bibliography

[1] V. Okhmatovski, M. Yuan, and R. Phelps, "Solver for modeling a multilayered integrated circuit with three-dimensional interconnects," Aug. 28 2012. US Patent 8,255,849.

[2] H. Ishikawa, "Optical multilayer structure, optical switching device, and image display," Sept. 6 2005. US Patent 6,940,631.

[3] E. Mombello, O. Trad, J. Rivera, and A. Andreoni, "Two-layer soil model for power station grounding system calculation considering multilayer soil stratification," *Electric power systems research*, vol. 37, no. 1, pp. 67–78, 1996.

[4] E. Szaraniec, "Fundamental functions for horizontally stratified earth," *Geophysical Prospecting*, vol. 24, no. 3, pp. 528–548, 1976.

[5] S. Zheng, R. Gholami, D. Isleifson, D. Barber, and V. Okhmatovski, "Analysis of scattering on arctic sea ice in c-band with layered medium formulation of surface volume surface electric field integral equation," in *2018 IEEE International Symposium on Antennas and Propagation & USNC/URSI National Radio Science Meeting*, pp. 1345–1346, IEEE, 2018.

[6] A. F. Peterson, S. L. Ray, R. Mittra, I. of Electrical, and E. Engineers, *Computational methods for electromagnetics*, vol. 2. IEEE press New York, 1998.

[7] C.-T. Tai, *Dyadic Green functions in electromagnetic theory.* Institute of Electrical & Electronics Engineers (IEEE), 1994.

[8] W. C. Chew, *Waves and Fields in Inhomogeneous Media (Electromagnetic Waves).* IEEE Computer Society Press, 1995.

[9] M. N. O. Sadiku, *Numerical Techniques in Electromagnetics with MATLAB, Third Edition.* Boca Raton, FL, USA: CRC Press, Inc., 3rd ed., 2009.

[10] L. Brekhovskikh, *Waves in layered media*, vol. 16. Elsevier, 2012.

[11] K. A. Michalski and J. R. Mosig, "Multilayered media green's functions in integral equation formulations," *IEEE Transactions on Antennas and Propagation*, vol. 45, no. 3, pp. 508–519, 1997.

[12] W. Chew, J. Zhao, and T. Cui, "The layered medium green's function—a new look," *Microwave and optical technology letters*, vol. 31, no. 4, pp. 252–255, 2001.

[13] Y. Chow, N. Hojjat, S. Safavi-Naeini, and R. Faraji-Dana, "Spectral green's functions for multilayer media in a convenient computational form," *IEE Proceedings-Microwaves, Antennas and Propagation*, vol. 145, no. 1, pp. 85–91, 1998.

[14] M. Aksun, "A robust approach for the derivation of closed-form green's functions," *IEEE Transactions on Microwave Theory and Techniques*, vol. 44, no. 5, pp. 651–658, 1996.

[15] J. R. Mosig and F. E. Gardiol, "Analytical and numerical techniques in the green's function treatment of microstrip antennas and scatterers," in *IEE Proceedings H (Microwaves, Optics and Antennas)*, vol. 130, pp. 175–182, IET, 1983.

[16] K. A. Michalski, "Extrapolation methods for sommerfeld integral tails," *IEEE Transactions on Antennas and Propagation*, vol. 46, no. 10, pp. 1405–1418, 1998.

[17] R. Golubovic, A. G. Polimeridis, and J. R. Mosig, "Efficient algorithms for computing sommerfeld integral tails," *IEEE Transactions on Antennas and Propagation*, vol. 60, no. 5, pp. 2409–2417, 2012.

[18] F. Ling and J.-M. Jin, "Discrete complex image method for green's functions of general multilayer media," *IEEE microwave and guided wave letters*, vol. 10, no. 10, pp. 400–402, 2000.

[19] L. Zhuang, Y. Zhang, W. Hu, W. Yu, and G.-Q. Zhu, "Automatic incorporation of surface wave poles in discrete complex image method," *Progress In Electromagnetics Research*, vol. 80, pp. 161–178, 2008.

[20] Y. P. Chen, W. C. Chew, and L. Jiang, "A novel implementation of discrete complex image method for layered medium green's function," *IEEE Antennas and Wireless Propagation Letters*, vol. 10, pp. 419–422, 2011.

[21] V. I. Okhmatovski and A. C. Cangellaris, "Evaluation of layered media green's functions via rational function fitting," *IEEE microwave and wireless components letters*, vol. 14, no. 1, pp. 22–24, 2004.

[22] V. N. Kourkoulos and A. C. Cangellaris, "Accurate approximation of green's functions in planar stratified media in terms of a finite sum of spherical and cylindrical waves," *IEEE transactions on antennas and propagation*, vol. 54, no. 5, pp. 1568–1576, 2006.

[23] A. Cangellaris and V. Okhmatovski, "Novel closed-form green's function in shielded planar layered media," *Microwave Theory and Techniques, IEEE Transactions on*, pp. 2225 – 2232, 01 2001.

[24] V. I. Okhmatovski and A. C. Cangellaris, "A new technique for the derivation of closed-form electromagnetic green's functions for unbounded planar layered media," *IEEE Transactions on Antennas and Propagation*, vol. 50, no. 7, pp. 1005–1016, 2002.

[25] L. B. Proekt and A. Cangellaris, "An approximation of the electromagnetic green's function of layered media with the source point considered as an independent variable," *IEEE transactions on magnetics*, vol. 40, no. 2, pp. 1037–1040, 2004.

[26] Y. Hua and T. K. Sarkar, "Generalized pencil-of-function method for extracting poles of an em system from its transient response," 1989.

[27] M. Yuan, T. K. Sarkar, and M. Salazar-Palma, "A direct discrete complex image method from the closed-form green's functions in multilayered media," *IEEE Transactions on Microwave Theory and Techniques*, vol. 54, no. 3, pp. 1025–1032, 2006.

[28] S. Ramo, J. Whinnery, and T. Van Duzer, *Fields and Waves in Communication Electronics*. Wiley-India, 1994.

[29] A. Cangellaris and L. Yang, "Rapid calculation of electrostatic Green's functions in layered dielectrics," *IEEE Transactions on Magnetics*, vol. 37, pp. 3133–3136, Sept. 2001.

[30] C. H. Edwards and D. E. Penney, *Differential Equations Computing and Modeling*. Upper Saddle River, NJ, USA: Prentice Hall Press, 4th ed., 2007.

[31] A. Polyanin, *Handbook of Linear Partial Differential Equations for Engineers and Scientists*. CRC Press, 2001.

[32] R. E. Collin, *Foundations for microwave engineering*. John Wiley & Sons, 2007.

[33] J.-M. Jin, *The finite element method in electromagnetics*. John Wiley & Sons, 2015.

[34] M. Abramowitz and I. A. Stegun, *Handbook of Mathematical Functions with Formulas, Graphs, and Mathematical Tables*. New York: Dover, ninth dover printing, tenth gpo printing ed., 1964.

[35] L. V. Ahlfors, *Complex analysis*. International series in pure and applied mathematics, New York, NY: McGraw-Hill, 3rd ed. ed., 1979.

Appendix A

Proof

We only need to prove Lemma 1.1 since Fourier-Bessel transform is essentially the two-dimensional Fourier transform of a circularly symmetric function. Moreover, the one-dimensional result can be readily generalized to two-dimensions. So the 1D case is proved afterwards. Given one-dimensional Fourier transform pair as

$$\tilde{f}(\omega) = \int_{-\infty}^{\infty} f(t) e^{-i\omega t} dt \tag{A.1}$$

$$f(t) = \frac{1}{2\pi} \int_{-\infty}^{\infty} \tilde{f}(\omega) e^{i\omega t} d\omega, \tag{A.2}$$

the problem and proof follow.

Problem: Consider two functions $f(t)$ and $g(t)$ having the same spectrum $\tilde{f}(\omega)$ and $\tilde{g}(\omega)$ after Fourier transform, prove $f(t) = g(t)$ for $\forall t$.

Proof. For $\forall t$,

$$f(t) - g(t) = \mathcal{F}^{-1}\{\tilde{f}(\omega) - \tilde{g}(\omega)\} = \mathcal{F}^{-1}\{0\} = \frac{1}{2\pi} \int_{-\infty}^{\infty} 0 \cdot e^{j\omega t} d\omega = 0 \tag{A.3}$$

□

Appendix B

Evaluation of Exponential Geometric Series in Sections 4.2.3.1 and 4.2.3.2

$$\begin{aligned}\sum_{k=-\infty}^{0} e^{-iaD} &= \sum_{k=-\infty}^{0} e^{-i\pi(\frac{z+z'}{d}-2k)D} = \sum_{k=-\infty}^{0} e^{-i\pi((z+z')D/d-2kD)} \\ &= e^{-i\pi(z+z')D/d}\sum_{k=-\infty}^{0} e^{i2\pi kD} = e^{-i\pi(z+z')D/d}\sum_{k=0}^{\infty} e^{-i2\pi kD} \\ &= \frac{e^{-i\pi(z+z')D/d}}{1-e^{-i2\pi D}}. \end{aligned} \tag{B.1}$$

In the similar manner, we have

$$\sum_{k=-\infty}^{0} e^{iaD} = \frac{e^{i\pi(z+z')D/d}}{1-e^{i2\pi D}}, \tag{B.2}$$

$$\sum_{k=1}^{\infty} e^{-iaD} = \sum_{k=1}^{\infty} e^{-i\pi((z+z')D/d-2kD)}$$

$$= e^{-i\pi(z+z')D/d} \sum_{k=1}^{\infty} \frac{e^{i2\pi D}}{1-e^{i2\pi D}} = \frac{e^{i\pi D(2-(z+z')/d)}}{1-e^{i2\pi D}}, \tag{B.3}$$

$$\sum_{k=1}^{\infty} e^{iaD} = \frac{e^{i\pi D((z+z')/d-2)}}{1-e^{-i2\pi D}}. \tag{B.4}$$